

DEPARTMENT OF THE AIR FORCE
HEADQUARTES, 603D REGIONAL SUPPORT GROUP (USAFE)
**European Office of Aerospace Research and Development
(EOARD)**

Grant SPC 02-4040, Order number FA8655-02-M4040

Awarded effective date 16 September 2002

Final Report

Summarizing all progress on the tasks outlined in the proposal

Contract title: **Investigation of chemical generation of atomic Iodine for COIL, and its testing in the supersonic COIL using a diode probe**

Investigators: **Otomar Špalek, Vít Jirásek, Miroslav Čenský,
Jarmila Kodymová**

Contractor: **Jarmila Kodymová
Department of Gas Lasers
Institute of Physics
Academy of Sciences of the Czech Republic
Na Slovance 2
182 21 Prague 8
Czech Republic**

Phone : +420 266052699

Fax: +420 286890265

E-mail: kodym@fzu.cz

Date of report submission: **16 January 2004**
**According to a modified Order for Supplies or services:
16 months after the grant award**

STATEMENT

- (1) **The Contractor, Institute of Physics of the Academy of Sciences of the Czech Republic, hereby declares that, to the best of its knowledge and believes, the technical data delivered herewith under Contract No. FA8655-02-M4040 is complete, accurate, and complies with all requirements of the contract.**
- (2) **I certify that there were no subject inventions to declare as defined in FAR 52.227-13, during the performance of the Contract No. FA8655-02-M4040.**

Date: 16 January 2004

Name and Title of Principal Investigator:

Dr. Jarmila Kodymová

Name and Title of Authorized Official:

Ing. Karel Jungwirth, DrSc.
Director of Institute of Physics AS

Content

Outline of planned tasks of the Contract No. FA8655-02-M4040

Introduction

1. The investigation of the COIL performance with chemically generated atomic iodine via atomic chlorine

- 1.1. Description of the reaction system
- 1.2. Modification of COIL device for injection of reactive gases
- 1.3. Results of investigation
 - 1.3.1. *Generation of atomic iodine in nitrogen flow (without $O_2(^1\Delta)$)*
 - 1.3.2. *Gain measurements with chemically generated atomic iodine*
 - 1.3.3. *Lasing with chemically generated atomic iodine*
 - 1.3.4. *Visual monitoring of $I_2(B-X)$ emission during lasing*
 - 1.3.5. *Beam patterns recording during lasing*
- 1.4. Conclusions from this investigation

2. The investigation of atomic iodine generation via atomic fluorine

- 2.1. Description of the reaction system
- 2.2. Experimental device and configuration
- 2.3. Results obtained with a longitudinal flow reactor
 - 2.3.1. *Conditions for I concentration profile measuring along the gas flow*
 - 2.3.2. *Effects of time intervals between NO and HI injection, and between HI injection and atomic I detection*
- 2.4. Results obtained with a transverse flow reactor
 - 2.4.1. *Conditions for I concentration profile measuring along the gas flow*
 - 2.4.2. *Measurements with injectors order NO-HI*
 - 2.4.3. *Measurements with injectors order HI-NO*
 - 2.4.4. *Temperature of the reaction mixture*
- 2.5. Conclusions from this investigation

3. Progress in mathematical modeling

- 3.1. Introductory remarks
- 3.2. 3-D modeling of atomic chlorine generation in the COIL subsonic channel
 - 3.2.1. *Description of the model*
 - 3.2.2. *Results of modeling*
 - 3.2.2.1. *Model case 1: the cold flow and low NO flow rate*
 - 3.2.2.2. *Model case 2: the reactive flow and low NO flow rate*
 - 3.2.2.3. *Model case 3: the non-reactive flow and excess of NO flow*
 - 3.2.2.4. *Model case 4: the reactive flow and excess of NO flow*
- 3.3. Modeling of chemical generation of atomic iodine
 - 3.3.1. *Results of penetration depths*
- 3.4. 1-D premix modeling of small signal gain in COIL with atomic iodine generation

4. References

5. Acknowledgement

6. Cost proposal

Outline of planned tasks o the Contract No. FA8655-02-M4040

1/ Investigation of the COIL performance with chemically generated atomic iodine via atomic chlorine

Goal: To get a laser generation with atomic iodine generated by the proposed chemical method on a reconstructed COIL device

2/ Generation of atomic iodine via atomic fluorine

Goal: To perform of the basic investigation on a small-scale device to prove a feasibility of this way of atomic iodine generation, and to compare the efficiency of atomic iodine generation in both reaction systems.

3/ Modeling of both reaction systems

Goal: To use the results of the 1-D modeling for the devices design, and a support and interpretation of experimental results. The advanced 3-D modeling will include fluid-dynamic and non-instantaneous mixing effects to describe more realistically a situation in the reaction system.

Introduction

The research on atomic iodine generation in the framework of this grant follows-up the previous contracts but the experimental work has moved up in the case of “chlorine” system from the small-scale devices to the supersonic COIL. The Iodine Scan Laser Diode Probe diagnostics was used for the parametric COIL testing. This diagnostics lent to our COIL Laboratory from the US AFRL at the Kirtland AFB was necessary for this investigation.

Results of the systematic investigation of atomic iodine generation via Cl atoms performed on the small-scale devices were summarized in the Final Report of the previous Contract SPC 00-4057 submitted to the USAF EOARD on 10 July 2002. Other results were recently presented in our papers with the Acknowledgement to the USAF EOARD.

1. The investigation of the COIL performance with chemically generated atomic iodine via atomic chlorine

1.1. Description of the reaction system

The interpretation of experimental results given below requires referring to the reactions that play more or less important role in the whole process of chemical generation of atomic iodine in the reactive COIL medium. Therefore this reaction system is described here briefly again even though it was included already in the previous EOARD reports. The atomic iodine generation runs through the two-step reaction process. First, atomic chlorine is formed in the reaction of

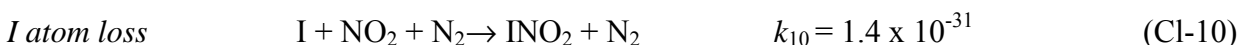
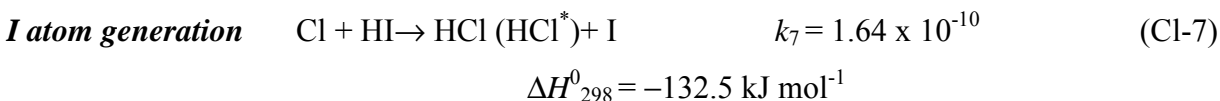
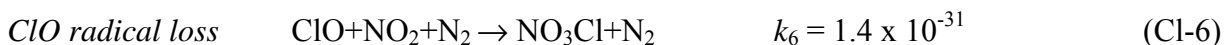
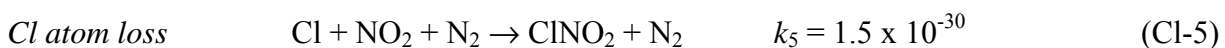
chlorine dioxide with nitrogen oxide, and then atomic chlorine reacts with hydrogen iodide. Each reaction step involves further a set of side production or loss reactions.



with Cl and ClO as the chain carriers. Individual steps:



Cl atoms prevail as a product of reaction (Cl-3) if initial concentration ratio of NO:ClO₂ is 2:1, while ClO radicals are mostly formed at the ratio 1:1.



Additional processes including primarily quenching reactions of singlet oxygen and excited atomic iodine should be also considered in a comprehensive kinetic model. According to a literature survey, ClO₂, NO, NO₂, HCl, and HI molecules quench O₂(¹Δ_g) only slightly because these quenching constants are comparable or lower than the rate constant for the O₂(¹Δ_g) self-quenching and pooling reactions (of the order of 10⁻¹⁷ cm³ molec⁻¹ s⁻¹). Since the concentration of these components in the reaction system is much lower than the O₂(¹Δ_g) concentration in a COIL medium, their quenching effect can be neglected. The rate constant for quenching of I^{*}, by HCl and HI is sufficiently low (of the order of 10⁻¹⁵ and 10⁻¹⁶, respectively) but the constants for ClO₂, NO and NO₂ are not available.

1.2. Modification of the COIL device for injection of reactive gases

The supersonic COIL device built in our laboratory consists of the singlet oxygen generator, diagnostic cell for detection $O_2(^1\Delta_g)$, $O_2(^1\Sigma)$, and residual Cl_2 , injectors of reacting gases for atomic I production, and the supersonic nozzle with 5 cm gain length. Singlet oxygen is supplied from the jet generator (of the horizontal cross-section of 6 x 4 cm and with the vertical gas outlet in the center) fed by helium-chlorine mixture. Subsonic channel of inner cross-section 5 x 0.95 cm and length 27 cm includes the throttle valve, ClO_2 injection tube, gate valve, diagnostic cell, NO and HI injectors. The gas flow is choked and expanded to the Mach number about 2. After a rapid expansion 1.5 cm downstream from the throat, the flow enters the expansion channel opened by 3°. The axis of the optical resonator was located 5.5 cm downstream of the nozzle throat having the cross-section of 5 x 0.67 cm. Injectors for all reacting gases were designed in accord with results of previous 1-D modeling of the above reaction system [1] and experimental investigation performed on small-scale reactors [1-3]. **Gaseous ClO_2 is injected** into the primary gas flow through a horizontal tube of 8 mm in diameter and with two rows of 0.7 mm holes. It was located in the center of the gas channel near the $O_2(^1\Delta_g)$ generator exit, and 18 cm upstream from the nozzle throat (see **Fig. 1**). **Nitrogen oxide and hydrogen iodide are injected** from two wall-side rectangular tubes located in the gas channel bottom and ceiling close to the nozzle throat. The cross-section of the injector body was shown in Fig. 27 of Final report [2]. Both NO and HI injectors contained one row of 0.7 mm-holes and one row of 0.5 mm-holes in each tube. The rows with 0.5 mm holes were placed 0.9 cm and 0.35 cm, respectively, upstream of the nozzle throat. The injectors heating don't need to be heated.

The Iodine Scan Diagnostics (ISD) with a narrow band tunable near infrared diode probe laser was used to monitor the gain or absorption of $I^* - I$ transition and I concentration in the resonator region. Gas temperature was calculated from the measured absorption-frequency curves by means of known procedure. The ISD probe beam moved either horizontally along the gas stream within 38 – 72 mm from the nozzle throat, or perpendicularly to the gas flow between the cavity bottom and ceiling.

Gaseous ClO_2 was produced on site by the reaction of chlorine with sodium chlorite [4]. Chlorine was diluted by nitrogen (in the ratio of 1:20 to 1:40) to assure, for safety reasons, the ClO_2 partial pressure below 13 kPa (100 torr) [5]. The generator with 2 liters of $NaClO_2$ solution

(40% (w/w)) could produce, e.g., $2 \text{ mmol s}^{-1} \text{ ClO}_2$, which was sufficient for about one hour's COIL operation. The NO/N₂ mixture (with 10 % NO), and HI/N₂ mixture (with 10 % or 5 % HI) were commercially available. The NO mixture was delivered from the Linde Comp., the HI gas from the H&S Chemical Co. Inc., USA. Initially HI was prepared in our laboratory from solid iodine, water and red phosphorus. Calibrated flow meters with a diaphragm orifice were used for measuring flow rate of the gases. Gas exiting the laser passed through a liquid nitrogen trap and then exhausted with a Roots pump of the capacity $0.83 \text{ m}^3 \text{ s}^{-1}$.

The COIL device was equipped with spectrophotometric detection of ClO₂. The ClO₂ content was measured from the absorption in the spectral range of 250 - 500 nm. Optical cell for this measurement was placed in the gas line between the ClO₂ generator and pressure-reducing valve. **Fig. 2** shows an example of measured spectrophotometric curve used for evaluation of ClO₂ concentration.

A continuous recording of the yellow “flame”, i.e. the emission of I₂(B-X) in the cavity downstream of the resonator was performed by the camcorder. These records helped to estimate qualitatively a penetration of the secondary gases (NO and HI) into the primary gas stream with O₂(¹Δ) and ClO₂, and the extent of atomic iodine recombination.

The operation of jet SOG was substantially improved after revealing the reason for a rather intensive BHP droplets escaping from our generator. It was caused by a leak between the BHP injector made of alkamide and stainless steel outlet tubes. A current reconstruction of the generator enables to operate the COIL for many experimental runs without a gas channel cleaning.

1.3. Results of investigation

1.3.1. Generation of atomic iodine in nitrogen flow (without O₂(¹Δ))

The effect of ClO₂, NO, and HI flow rates on atomic iodine production was studied first. A concentration of atomic iodine measured by ISD in the center of the COIL cavity (55 mm from the nozzle throat) in dependence on the NO flow rate is shown in **Fig. 3**. The yield of atomic iodine related to HI increased in this measurement from 14 % to 89 % when the NO:ClO₂ ratio increased from 1 to 1.8. The maximum yield (90 – 100 %) was attained at NO:ClO₂ \cong 2. This value corresponds with the stoichiometric ratio of reaction (Cl-1). **Fig. 4** shows the effect of HI flow rate on the I concentration measured also in the center of the cavity. This directly proportional dependence corresponds with the first order of reaction (Cl-7) related to HI. An important result of these experiments was obtained when the ISD diode probe beam detected the

I concentration along the gas flow through the cavity. The I concentration was nearly constant, which is illustrated in **Fig. 5**. This indicates a low rate of atomic iodine recombination in this region in spite of the presence of NO₂ molecules (reactions (C-10) and (C-11)). These measurements represented by Figs. 2 – 4 were performed with the primary gas containing ClO₂/N₂ mixture only (without the primary He), and the system was exhausted with the pump of smaller capacity (0.278 m³ s⁻¹).

The atomic iodine concentration recorded across the cavity (i.e., in the direction perpendicular to the gas stream) by means of ISD probe varied much more than along the cavity. It was strongly affected by the flow rates of the primary gas and injected secondary gases NO and HI. Mapping the I concentration across the cavity could optimize this mixing process. This is demonstrated in **Fig. 6**. These measurements were made with primary helium and the pump of the capacity 0.83 m³ s⁻¹. The concentration profiles of atomic iodine were recorded in the cavity 55 mm from the nozzle throat for different flow rates of ClO₂, NO and HI in the approximate ratio of 1 : 2 : 1. In case of the lowest NO and HI flow rates, the penetration of these gases into the main gas flow was insufficient, which resulted in the concentration minimum of atomic iodine in the cavity center (curve 1). This minimum gradually disappeared with increasing NO and HI flow rates and a parabolic concentration profile was obtained for the highest flow rates of these reactants.

These measurements proved that the concentration of atomic iodine and its distribution in the COIL supersonic cavity (at M ~ 2) are satisfactory for the supersonic COIL operation, and that atomic iodine can be produced by this chemical way with the high yield (80 - 100 % related to HI or ClO₂).

The measured ISD data were used also for the evaluation of gas temperature. An example of the temperature profile across the cavity is shown in **Fig. 7** (the corresponding iodine concentration profile is illustrated by the curve 3 in Fig. 5). Despite of the exothermic effect of reactions (CI-1) and (CI-7), the temperature in the cavity center was relatively low (~230 K) due to the isentropic gas flow expansion.

1.3.2. Gain measurements with chemically generated atomic iodine

In these measurements, the primary gas flow consisted usually (after the ClO₂ admixing) of 80 mmol/s He_{prim}, 15 mmol/s O₂(¹Δ), 9 mmol/s O₂(³Σ), 3 mmol/s of residual Cl₂ and 0.9 – 2.3 mmol/s ClO₂ in the mixture with N₂ (1:10). The O₂(¹Δ) yield was about 60 % at the total pressure of 8 kPa in the generator. The pressure in the gas channel upstream of the nozzle throat was 3 – 4 kPa.

In the first experiment, zero gain in the cavity center was obtained with the same ClO_2 , NO and HI flow rates like in Fig. 6 (curve 1) where the gain was measured in the gas flow without singlet oxygen, residual chlorine and He_{prim} . The zero gain in the cavity center was explained by a low penetration of NO and HI flows into the more dense primary gas flow and its higher overall flow rate due to additional presence of oxygen and residual Cl_2 . The calculations also proved that the relative penetration factors [6] for both NO and HI flows were insufficient ($\pi_r \sim 0.7$). A small value of gain ($0.15 \% \text{ cm}^{-1}$) was measured in this experiment 4 mm above or below the cavity centerline, and the gain was constant along the flow (**Fig. 8**). This proved that neither excited atomic iodine or singlet oxygen was quenched significantly by some species in the gain region.

To get the gain also in the cavity center, the flow rates of secondary gases were increased to increase their penetration. It was however found that the flow rates of NO and HI that were sufficient to get a uniform concentration profile of atomic iodine in the system without $\text{O}_2(^1\Delta)$ (curve 2 in Fig. 6) were not sufficient for attaining a homogeneous gain profile in $\text{O}_2(^1\Delta)$ flow (see **Fig. 9**), due to a higher density and flow rate of the primary gas. A uniform gain distribution was achieved only at still higher flow rates of secondary gases (**Fig. 10**).

Some measurements were performed with a transonic admixing of HI in order to reduce a possible quenching of excited atomic iodine upstream of the nozzle throat. A distance between two HI injector tubes was reduced to 6.5 mm to create there a critical cross-section. It was found that the gain distribution across the COIL cavity was less homogeneous than in the case of subsonic HI admixing (at the same flow rates of primary and secondary gases). This was explained by a lower penetration of HI flow at the transonic admixing.

The maximum gain of $0.30 - 0.35 \%/\text{cm}$ achieved at subsonic HI injection can be considered as a rather good result for application of this quite new method of atomic iodine generation in the COIL. This value is lower in comparison with the optimum value attainable in the conventional COIL devices using molecular iodine as the I atoms source. To compare the measured average gain of $0.28 \%/\text{cm}$ with the theoretical value, we performed the following estimation. The gain, α_{3-4} , was calculated from the equation [7]

$$\alpha_{3-4} = (7/24) \sigma_{3-4} [(2K_{eq}+1)\eta_{\Delta} - 1] / [(K_{eq}-1)\eta_{\Delta} + 1] c_I, \quad (\text{CI-12})$$

where σ_{3-4} is the cross-section of the 3-4 transition in iodine atom, K_{eq} the equilibrium constant of the energy pumping, η_{Δ} the $\text{O}_2(^1\Delta)$ yield, and c_I the atomic iodine concentration in the active

medium. The gain of 0.36 %/cm was calculated using the value of $\sigma_{3-4} = 1.3 \times 10^{-17} \text{ cm}^2$, the equilibrium constant, $K_{eq} = 0.75 \exp(401.4/T)$ ($T = 240 \text{ K}$), the $\text{O}_2(^1\Delta)$ yield of 60 %, and $c_I = 6 \times 10^{15} \text{ cm}^{-3}$ measured in the COIL cavity without $\text{O}_2(^1\Delta)$. The slightly lower measured gain values could have the following explanations. The suggested method of atomic iodine generation in COIL presupposed the low rate constant for $\text{O}_2(^1\Delta)$ quenching by HI molecule. This constant, $k_{HI} < 2 \times 10^{-17} \text{ cm}^3/\text{s}$, was obtained from measurements performed in the mixture of HI and singlet oxygen produced by a microwave discharge in pure oxygen [8]. We verified this kinetics by introducing HI into the stream of $\text{O}_2(^1\Delta)$ produced in the jet generator. In this measurement, two unexpected phenomena were observed. The ground state of atomic iodine with the concentration $c_I \sim 3.9 \times 10^{14} \text{ at}/\text{cm}^3$, and the high gas temperature 330 K were detected by the ISD measurement in the laser supersonic cavity. This temperature was by about 100 K higher than with the complete $\text{O}_2(^1\Delta)$ – ClO_2 – NO – HI reaction system under similar conditions. These phenomena could not be ascribed to the reaction of the residual chlorine with HI because of the small rate constant [9] but they could be explained for example by the reaction



This reaction might be accelerated by some component of the reaction medium (in the difference from the system in [8]). The presence of HO_2 radical, which strongly quenches $\text{O}_2(^1\Delta)$ ($k_{\text{HO}_2} = 3.3 \times 10^{-11} \text{ cm}^3/\text{s}$) [10] could explain the high temperature due to the heat release in the $\text{O}_2(^1\Delta)$ quenching process. A significantly lower temperature (175 – 225 K) measured with the complex reaction system $\text{O}_2(^1\Delta)$ – ClO_2 – NO – HI could be explained by a lower concentration of HO_2 radical due to its loss in the fast reaction with NO ($k_{\text{NO}} = 8.1 \times 10^{-12} \text{ cm}^3/\text{s}$) and/or Cl atoms ($k_{\text{Cl}} = 4.1 \times 10^{-11} \text{ cm}^3/\text{s}$) [11], [12]. The reaction (Cl-13) producing HO_2 radical was, however, neither found in the literature nor verified experimentally so far. The described hypothesis is not in contradiction with the measured nearly constant gain along the flow (see Fig. 8) because of all HI could be consumed before this region (by (Cl-7) and (Cl-13)). The lower measured gain vs. gain calculated from (Cl-12) may be caused not only by a partial consumption of $\text{O}_2(^1\Delta)$ in reaction (Cl-13), but also by a higher cavity temperature or lower rate of atomic I production in $\text{O}_2(^1\Delta)$ presence. No significant difference in the cavity temperature was however found by the ISD measurements with or without $\text{O}_2(^1\Delta)$ in the primary flow. Laser experiments performed at full penetration of secondary gases has shown that the optimum laser power was achieved at about the same ratio of reacting gases ($\text{ClO}_2 : \text{NO} : \text{HI} \cong 1:2:1$) as for optimal production of

atomic iodine in $O_2(^1\Delta)$ absence. This shows that the presence of $O_2(^1\Delta)$ does not affect substantially the kinetics of atomic iodine production.

The gas temperature in this COIL system was comparable with temperature typically measured in the COIL devices with molecular iodine as I precursor [13, 14].

1.3.3. Lasing with chemically generated atomic iodine

Effect of NO flow rate

In the experiments with constant ClO_2 flow rate and $n_{NO} < n_{ClO_2}$, the laser power increased approximately in direct proportion to NO flow rate. The maximum power was achieved at the ratio $NO:ClO_2 \geq 2$. The value 2 agrees with the stoichiometric ratio following from reaction (Cl-1) and corresponds to the maximum measured rate of atomic iodine formation (see chapter 1.3.1.). An excess of NO over stoichiometry (up to $NO:ClO_2 = 3.3$) had no negative effect on laser power. The output mirror transmittance was 0.9 % and the back mirror transmittance 0.1 %.

Effect of ClO_2 and HI flow rate

Fig. 11 shows the dependence of laser power on HI flow rate at different production rates of Cl atoms (or ClO_2 and NO flow rate, respectively). An increase in laser power with increasing HI flow rate can be explained by increasing concentration of iodine atoms available for lasing (see eq. (Cl-12)). The maximum power in this figure was achieved at about 2.5 mmol/s HI apart from ClO_2 and NO flow rates. This rather high HI flow rate (in comparison with the ClO_2 flow rate) is quite consistent with the observed increase in the average gain by increasing the HI flow rate over the corresponding ClO_2 flow rate (e.g. from 1.25 to 2 mmol s^{-1} HI at 1.33 mmol s^{-1} ClO_2 – compare Figs. 9 and 10). This is ascribed to a sufficient HI penetration. A slight decrease in laser power was observed with the excessive HI, which could be explained by the course of reaction (Cl-13) resulting in the formation of HO_2 radical. This radical can deactivate $O_2(^1\Delta)$ lowering thus its extractable energy. The described decrease in power is not too strong. For example, the P_L remained constant at the HI flow increase from 1.9 to 2.3 mmol s^{-1} (at 1.5 mmol s^{-1} ClO_2 + 3.3 mmol s^{-1} NO, which corresponds to the production rate of Cl atoms < 1.5 mmol s^{-1}). The power of 390 W was measured in this case at 40 mmol s^{-1} Cl_2 loaded into the generator. This demonstrates that the effect of HO_2 radical on $O_2(^1\Delta)$ quenching is limited. The maximum power was attained for 1 and 1.5 mmol/s ClO_2 and corresponding NO flow rate in the ratio about 1 : 2. The lower laser power measured for smaller ClO_2 flow rate (0.6 mmol/s) was caused probably by a lower production rate of atomic chlorine and consequently iodine. A slightly lower

power for the highest flow rates (2.2 mmol/s ClO₂ + 4.2 mmol/s NO) could be ascribed to the fast quenching of I^{*} by Cl atoms formed in excess over HI ($k_{Cl} \sim 10^{-10} \text{ cm}^3 \text{ s}^{-1}$).

Effect of HI concentration

In further experiments, the 5 % mixture of HI in nitrogen was used instead of 10 % mixture in order to attain a higher HI penetration. This resulted in the laser power more than twice higher at the same HI flow rate (compare curve 1 in **Fig. 12** and curve labeled Δ in Fig. 11, the region 0 to 1 mmol s⁻¹ HI). A decline of the line slope in the region above 1.1 mmol s⁻¹ HI can be explained by a limited rate of atomic chlorine production.

Effect of water vapor

Effect of water vapor coming from the ClO₂ flow is also shown in **Fig. 12**. The curve 1 was measured with the ClO₂+N₂ mixture that was injected into the subsonic COIL channel without previous water trapping; the curve 2 was measured with the ClO₂ mixture cooled to 3°C. It was estimated that the water vapor pressure in the cooled flow was more than 4 times lower. In spite of this, the curves 1 and 2 are nearly identical which means that water originating from the ClO₂ generator had negligible effect. Therefore, the ClO₂ gas was not cooled in further experiments. The curve 3 in Fig. 12 was obtained at the same flow rates of reacting gases, but the transmittance of the output mirror was higher ($T_1 = 1.4 \%$) than in other measurements ($T_1 = 0.9 \%$).

Effect of primary He

The output power could be rather affected by He_{prim} flow rate in O₂(¹Δ) generator. **Tab. 1** shows an increasing laser power with increasing He flow rate. The data were measured with 31 mmol s⁻¹ Cl₂ input to the jet SOG, and 2.2 mmol s⁻¹ ClO₂, 4.3 mmol s⁻¹ NO, and 1.6 mmol s⁻¹ HI.

Table 1

He _{prim} , mmol s ⁻¹	82	98	124	131
P _L , W	255	275	300	300
P _{gen} , kPa	9.2	10	11	11.9

The observed positive effect of higher He_{prim} flow rate was ascribed to a lower O₂(¹Δ) loss in the jet SOG, which was confirmed also by calculations. At 82 mmol s⁻¹ He_{prim}, 32 % of O₂(¹Δ) of its total production was lost in the subsonic region (upstream of the nozzle throat), while only 26 %

was lost at $131 \text{ mmol s}^{-1} \text{ He}_{\text{prim}}$. In the experiment with a higher chlorine flow rate ($40 \text{ mmol s}^{-1} \text{ Cl}_2$, $1.5 \text{ mmol s}^{-1} \text{ ClO}_2$, $4.9 \text{ mmol s}^{-1} \text{ NO}$, and $2 \text{ mmol s}^{-1} \text{ HI}$), the power was 380 W at $60 \text{ mmol s}^{-1} \text{ He}_{\text{prim}}$, and 430 W at $100 \text{ mmol s}^{-1} \text{ He}_{\text{prim}}$. Further increase in He flow rate had no positive effect.

Effect of chlorine

The laser power substantially increased linearly with increasing Cl_2 flow rate up to 31 mmol s^{-1} in the generator. With its further increase up to 40 mmol s^{-1} , the power grew much slower (by 5 to 13 % only), which was caused very probably by an increasing loss of $\text{O}_2(^1\Delta)$ in the generator. The calculated loss of $\text{O}_2(^1\Delta)$ increased from 24 % to 36 % due to a generator pressure increase. The chemical efficiency dropped from 13.5 % to 11.5 %. An improvement in the chemical efficiency at higher Cl_2 flow rates is anticipated in the newly fabricated generator that will have a larger cross-section of the gas outlet channel.

Comparison with the Simplified Saturation Model

The maximal laser output power of 430 W attained by experiments was compared with the value calculated from the simplified saturation model for the power extraction in the COIL [15]. For our cavity geometry, a rather good agreement between the theory and experiment was attained for the following parameters: $40 \text{ mmol s}^{-1} \text{ Cl}_2 + 90 \text{ mmol s}^{-1} \text{ He}_{\text{prim}}$ flow rates, 0.85 chlorine utilization, 0.6 $\text{O}_2(^1\Delta)$ yield at plenum, 0.3% cm^{-1} small signal gain, 200 K cavity temperature, $9 \times 10^{14} \text{ cm}^{-3}$ atomic iodine concentration, 900 m/s gas velocity, 0.7 % and 0.3 % mirror transmissions, negligible distributed non-saturable loss, 0.0015 mirror scattering loss, and 0.01 diffraction loss. It can be supposed that some increase in laser power could be achieved either by an increase in the gain or by reducing the mirror scattering loss.

1.3.4. Visual monitoring of $\text{I}_2(\text{B-X})$ emission

Emission intensity of $\text{I}_2(\text{B-X})$ radiation was monitored by the camcorder in the supersonic region (downstream of the resonator). A rather low intensity was observed in the middle of cavity when only HI was introduced into the $\text{O}_2(^1\Delta)$ stream. It was found by the ISD measurements that the ground state atomic iodine was mainly in this region (see chapter 1.3.2.). The absence of higher amount of I^* atoms was explained by the formation of HO_2 radical that quenches effectively $\text{O}_2(^1\Delta)$. The $\text{I}_2(\text{B-X})$ radiation intensity was much stronger in boundary layers where the gas velocity was lower, recombination of atomic iodine to I_2 occurred, and residual $\text{O}_2(^1\Delta)$ could excite $\text{I}_2(\text{X})$ to $\text{I}_2(\text{B})$ state (**Fig. 13**). In the case of simultaneous HI and NO

injection into the $O_2(^1\Delta)$ stream (without ClO_2), the $I_2(B-X)$ emission both in the main flow and the boundary layers was much weaker (**Fig. 14**). This was explained by the fast reaction of radical HO_2 with NO ($k_{NO} = 8.1 \times 10^{-12} \text{ cm}^3/\text{s}$), which reduces the $O_2(^1\Delta)$ quenching by HO_2 . The undesirable effect of HO_2 radical on $O_2(^1\Delta)$ is still more suppressed when atomic chlorine is present in the reaction system that reacts with HO_2 still faster (see chapter 1.3.2). In the complete reaction system for atomic iodine production ClO_2 - NO - HI in $O_2(^1\Delta)$, the emission intensity in the boundary layers was much weaker than the intensity in the cavity center (**Fig. 15**). The chlorine flow rate had no remarkable effect on the yellow radiation in the channel (**Fig. 15 a,b**). A more intensive yellow flame in the main flow was observed at higher HI flow rate. In this case, a central region containing prevalingly $O_2(^1\Delta)$ and HI was probably formed with a lack of Cl atoms. An extreme yellow radiation was observed at high HI and low NO flow rate where a central region with HI and without Cl atoms was formed **Fig. 16**.

1.3.5. Beam patterns

Beam patterns were recorded on a thin plywood substrate distant from the outcoupling mirror by 1.1 m. In optimal conditions, they had a roughly rectangular shape with “lens-type” upper and lower sides 63 ± 2 mm long and 22 mm high (**Fig. 17**). The pattern shape was affected mainly by the gain (i.e. by the primary energy of $O_2(^1\Delta)$ and concentration of generated atomic iodine), and the transmittance and quality of mirrors. The pattern was usually shorter (20–30 mm) at a lower power, which was caused by either a low gain or higher optical losses. **Fig. 18** shows a pattern example obtained with an impaired output mirror. By turning this mirror (which caused probably a shifting the impaired region of the mirror to a non-optical region), the power increased remarkably ($120 \rightarrow 330 \text{ W}$), which reflected also a substantially longer shape of the pattern (**Fig. 19**). With the increase in chlorine flow rate (from 32 to 40 mmol s^{-1}) at the same flow rate of He_{prim} and other gases, the power increased up to 360 W, and the beam pattern showed a slight beam inhomogeneity (**Fig. 20**). At higher He_{prim} flow rate, the power was also higher (390 W) and the beam pattern became more homogeneous (**Fig. 21**). A low HI flow rate at simultaneous high He_{prim} flow rate caused a low HI penetration, which resulted in a pattern with two narrow horizontal strips (see **Fig. 22**). **Fig. 23** shows a relatively uniform pattern at the same ClO_2 and NO flow rates but with higher HI and lower He_{prim} flow rates. This reflects a significant effect of homogeneity of HI in the flow. Shape of the beam pattern (see e.g. **Fig. 24**) as well as the power (see Fig. 10) was not affected by the ClO_2 flow rate in the range of 1.0 – 1.8

mmol s⁻¹ (at NO/ClO₂ ~ 2, and 2 – 3 mmol s⁻¹ HI). The pattern was constricted at the both ends (Fig. 25) and the power was lower by 20%.

2.3. Conclusions from this investigation

The investigation of the COIL operation including atomic iodine generated by the new chemical method was performed. Atomic iodine was produced by the reaction of hydrogen iodide with chemically formed chlorine atoms. This process was studied in the COIL cavity either in the absence or presence of singlet oxygen. In the absence of O₂(¹Δ), the yield of atomic iodine was very high (80 to 100%) in optimized experimental arrangement and at the NO / ClO₂ ≥ 2. The HI / ClO₂ ratio must be at least 1 and full penetration of HI stream into the primary flow must be assured. The concentration of generated atomic iodine along the gas flow through the laser cavity was very stable, indicating a low rate of iodine atoms recombination. On the other hand, the concentration of atomic iodine varied across the COIL cavity very much, which was affected by penetration of the secondary gases (NO, HI) into the primary gas flow.

In the O₂(¹Δ) flow, the maximum gain of 0.35 %/cm was attained. The gain was also nearly constant in the flow direction, which revealed an absence of any strong quencher of atomic iodine (or singlet oxygen) in the gain region. A rather uniform gain across the cavity was achieved by adjusting an optimum penetration of secondary gases given by the flow rate ratio of primary and secondary gases. The measured gain was about twice lower in comparison with the calculated value. It was explained by some loss of singlet oxygen before the gain region due to a possible formation of HO₂ radical in reaction (Cl-13). It was found that the effect of this reaction is substantial in the system HI - O₂(¹Δ) without NO and Cl atoms in the system. The effect of HO₂ radical on the gain is much weaker in the system with NO and Cl atoms owing to fast reactions of these species with HO₂ radical.

In laser experiments, the maximum output power of 430 W was attained for 40 mmol s⁻¹ Cl₂, the flow rate of ClO₂ in the region of 1 – 1.8 mmol s⁻¹, and the NO flow rate in the corresponding ratio of NO/ClO₂ ≥ 2. The optimum HI flow rate should be HI/ClO₂ ≥ 1. A sufficient penetration into the primary flow should be further attained. On the other hand, the region of their optimum flow rates is rather broad. By increase in He_{prim} in some region of the flow rate, the power can be also increased due to a lowering the O₂(¹Δ) loss in the generator.

It was further shown that water coming from the ClO₂ generator had no effect on laser power.

The calculation of the laser power from the simplified saturation model has shown a reasonable agreement with the measured power for the following parameters: 0.85 chlorine utilization, 0.6 O₂(¹Δ) plenum yield, 0.3 %/cm small signal gain, 0.0015 mirror scattering loss, and 0.01 diffraction loss.

The recording of the I₂ (B-X) radiation in the gas channel, and the beam patterns helped to understand the processes taking place in the COIL with chemical generation of atomic iodine.

It was the first time when the gain and laser output power was achieved in the COIL with atomic iodine generated by the proposed method. The advantage of this way (in comparison with the conventional I₂ dissociation) is an easier control of the atomic iodine flow rate, measuring the I₂ concentration is avoided, as well as the heating of the iodine system.

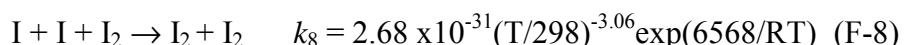
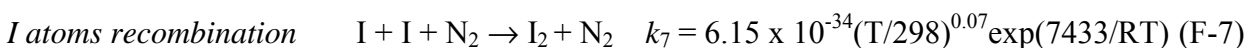
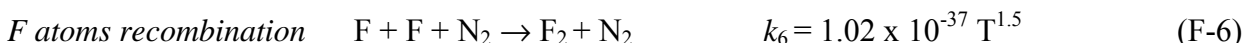
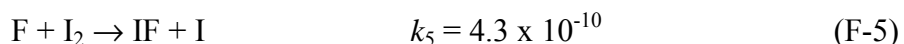
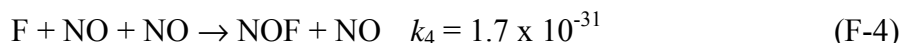
Plans for the next investigation:

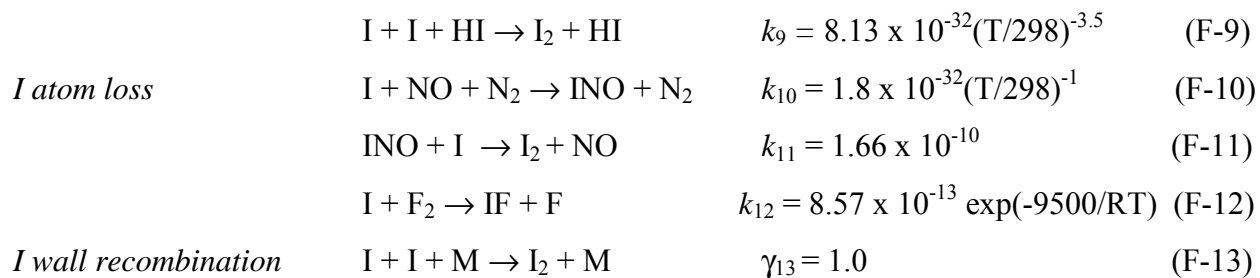
To increase the power by increasing the flow rate of O₂(¹Δ) into the laser, which we expect with the modified jet SOG. This new version will have a larger cross-section of gas channel at the generator exit. As the quality of the resonator mirrors was proved to be crucial, we ordered purchasing of new mirrors. Further measurements of the gain by the ISD probe will be performed to understand better the kinetics of the system.

2. The investigation of atomic iodine generation via atomic fluorine

2.1.1. Description of the reaction system

The kinetic package of the following reactions with relevant rate constants in cm³molecule⁻¹s⁻¹ and cm⁶molecule⁻²s⁻¹, respectively, was used for the 1-D and 2-D modeling of investigated reaction system and the interpretation of experimental results.

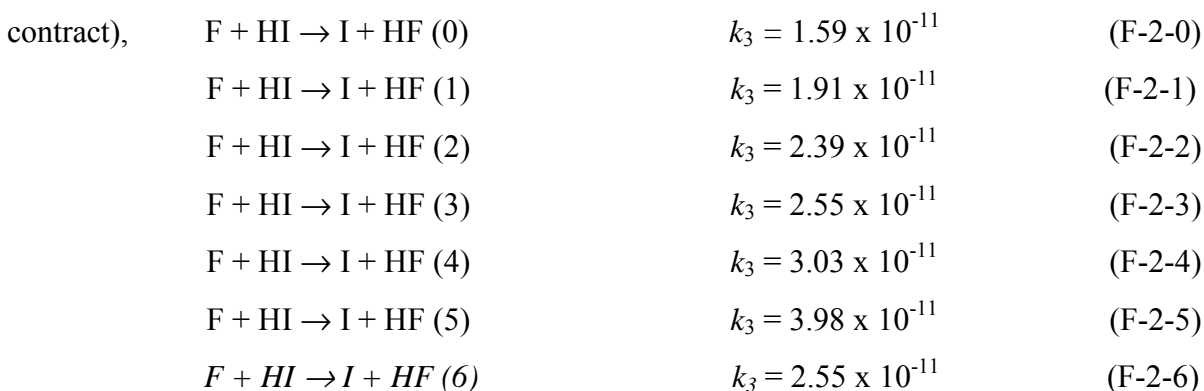




A heat effect of the individual reactions may be assessed from their reaction enthalpies listed below

$\Delta H_{r1} = - 77.22 \text{ kJ mol}^{-1}$	$\Delta H_{r7} = - 151.1 \text{ kJ mol}^{-1}$
$\Delta H_{r2} = - 273.3 \text{ kJ mol}^{-1}$	$\Delta H_{r8} = - 151.1 \text{ kJ mol}^{-1}$
$\Delta H_{r3} = - 236.0 \text{ kJ mol}^{-1}$	$\Delta H_{r9} = - 151.1 \text{ kJ mol}^{-1}$
$\Delta H_{r4} = - 236.0 \text{ kJ mol}^{-1}$	$\Delta H_{r10} = - 263.37 \text{ kJ mol}^{-1}$
$\Delta H_{r5} = - 129.8 \text{ kJ mol}^{-1}$	$\Delta H_{r11} = - 112.49 \text{ kJ mol}^{-1}$
$\Delta H_{r6} = - 158.78 \text{ kJ mol}^{-1}$	$\Delta H_{r12} = - 122.13 \text{ kJ mol}^{-1}$

The reaction enthalpy of reaction (F-3) given in the list above relates to HF molecule that is in the ground state. This species is however predominantly in vibrationally excited states, so we calculated the effective reaction enthalpy from the rate constants published for this reaction considering the vibrational distribution within HF (at 300 K,) (see interim Report 002 of this



and from the energy calculated for individual vibration states. The calculated effective value of the reaction enthalpy for reaction (F-2) thus was 229.74 kJ mol⁻¹.

2.2. Experimental device and configuration

This investigation was performed in small-scale devices of different configurations. One configuration employed a longitudinal cylindrical flow reactor (further designated as the reactor 1) that had axially movable injectors for NO and HI injection. The configuration enabled to vary

a time interval between NO and HI injection, and between HI injection and atomic I detection in the optical cell located outside the reactor. The second configuration used a reactor of rectangular inner space (further designated as the reactor 2), a part of which was the optical cell for atomic iodine detection, which enabled to shorten a time delay between I formation and its detection, and mainly to measure a concentration profile of atomic iodine along the gas flow through the detection cell. A cross-section of the reactor 1 is schematically shown in **Fig. 26**. This reactor is made of stainless steel tube of 10 mm i.d. Two injectors are inserted in the reactor bends for admixing the secondary gases (NO/N₂ mixture with 10 % NO, and HI/N₂ mixture with 8 % HI) into the primary gas flow (F₂/N₂ mixture with 10 % F₂). The NO injection was inserted into the position 1 or 2, and the remaining bend was plugged. The injectors were made of stainless-steel tube of 5 mm in o.d with two or three rows of openings. The NO injector contained 24 openings of 0.4 mm i.d., and the HI injector contained 16 openings of the same diameter. In most experiments, the NO gas was injected through the injector #1 (in position 1 or 2), and the HI gas through the injector #2. A cross section of the reactor 2 is shown in **Fig. 27**. The reactor consists of the delta-shaped channel for the primary gas introduction into the rectangular cavity of the reactor, the NO injector inserted in the cavity center perpendicularly to the primary gas flow, and two HI injectors embedded in the upper and bottom walls of the cavity. A part of the cavity was equipped with two side windows used for optical detection of formed atomic I and recording its concentration profile along the cell. The reactor cavity was 25 mm wide and 8 mm high. The F₂/N₂ mixture was introduced through a tube with the flange 1 extended in the delta-shaped channel 2 up to a width of 25 mm. The NO injector 3 contained two rows of holes of 0.4 mm i.d. with 23 holes in each row. A distance between nearby holes was 1 mm. Both rows of holes were oriented in vertical direction (up and down). Each HI injector 4 contained 9 holes of 0.4 mm i.d. in one row. By turning the HI injectors, a time delay between NO and HI injection could be varied to a certain extent. In some experiments, the order of NO and HI injection was reversed to study the effect of mixing order on the kinetics of I generation. The probe beam of ISD diode laser passed through two side wedge-shaped windows of the cell perpendicularly to the gas flow. The ISD probe beam emitter/detector unit was mounted on the assembly of motorized linear positioning equipment controlled by PC. In this configuration, the probe beam could move along the cell so that its distance from the HI injector varied between 12 mm and 60 mm (dotted area in Fig. 27). The gas temperature was measured by a jacketed Ni-CrNi thermocouple 6 (1 mm o.d.) that was inserted perpendicularly to the gas flow, 5 mm downstream of the end of the windows.

The local flow rate of atomic iodine n_I (in $\mu\text{mol s}^{-1}$) was calculated from the local concentration of atomic iodine, c_I , (evaluated from the ISD measurement for the centerline of the gas channel). It was calculated by the relation

$$n_I = c_I V / N_A \quad . \quad (\text{I})$$

N_A is the Avogadro number and V is a volumetric flowrate of gas mixture through the detection cell, which was evaluated from the modified equation of state

$$V = n_t R T / P \quad . \quad (\text{II})$$

n_t is the total molar flow rate representing the sum of molar flow rates of all gas components, T is the gas temperature, and P is the pressure measured in the detection cell. A typical overall pressure of the gas mixture ranged between 1 and 2.5 kPa.

The rate constant of reaction



had to be measured. In these measurements F_2/N_2 mixture (10 % F_2) was introduced into the reactor 2 as the primary flow and HI/N_2 mixture (8 % HI) through two injectors (4 in Fig. 27). Argon ion laser was used to determine concentration of molecular iodine from its light absorption. Its beam passed through two optical cells that were placed downstream of the reactor. It was calculated that the gas mixture reached these cells 3.2 ms and 10.5 ms after HI admixing.

2.3. Results obtained with the longitudinal flow reactor

2.3.1. Effect of flow rates of reacting gases at constant time intervals between NO and HI injection and between HI injection and atomic I detection

The first experiments were performed with nearly instantaneous injection of NO and HI into the F_2/N_2 flow (a time interval of 0.027 ms only was between injections of both secondary gases). To have a minimum time delay between injections of both gases followed from the results of our previous 1-D modeling of this reaction system, and was explained by a minimum loss of fluorine atoms (formed in (F-1)) due to their immediate reaction with HI molecules present in their vicinity (reaction (F-2)). The rate of I production (expressed in I molar flow rates) in dependence on the F_2 flow rate is shown in **Fig. 28** for two time intervals between HI injection and atomic I detection ($\tau_{\text{HI-ISD}}$). The curves 1 and 2 in Fig. 28 were recorded simultaneously in two detection cells. In the curve 1, the I flow rate initially increased with increasing F_2 flow rate due to an increasing rate of F atom formation (reaction (F-1)), and after reaching a maximum it declined. This decline could be explained by the effect of reaction

between formed atomic I and F₂ molecules present in excess in the reaction mixture (reaction (F-12)). Atomic F formed also in this reaction could sequentially produce another atomic I through reaction (F-2) provided that a sufficient concentration of HI is in the reaction system. This was proved by the next experiments with the HI flow rate 2.8 times higher than in Fig. 28 (at the same NO flow rate). No decrease in atomic I flow rate was then observed with increasing F₂ flow rate, even if the F₂ flow rates were rather high (190 – 230 $\mu\text{mol/s}$ F₂).

Fig. 29 shows the dependence of atomic I production on NO flow rate at constant F₂ and HI flow rates and for the same injection configuration. The curve 1 measured also for $\tau_{\text{HI-ISD}} = 2.7$ ms had a similar character as in Fig. 28. The observed initial increase in atomic I production can be ascribed to the increasing rate of reaction (F-1), and a following diminishing was probably caused by a growing effect of the loss-reactions (F-3) and (F-4). A maximum production of atomic I was attained in rather wide range of molar flow ratios of NO/F₂ (from 0.8 to 2.3). This is caused probably by two effects: the effect of NO flow rate on the rate of I formation itself, and the effect of shifting the region of I formation with increasing NO flow rate closer to the NO injection.

A dependence of atomic I production on the HI flow rate (**Fig. 30**) had a similar character like the dependences on F₂ and NO flow rates, respectively. The increasing HI concentration resulting in an increase of reaction rate of the reaction (F-2) caused an initial increase in atomic I production, while declining part of the curve at higher HI flow rates was induced probably by shifting the maximum production of atomic I closer to the HI injection. This explanation was supported by measuring of dependence of atomic I flow rate, recorded in two cells, on the total pressure.

2.3.2. Effects of time intervals between NO and HI injection, and between HI injection and atomic I detection

The next series of experiments was performed with several different positions of NO and HI injectors to study the effect of time interval between NO and HI injection on I production. By prolonging this interval up to 0.34 ms, no significant effect was observed at the same NO and HI flow rates like in Fig. 28 where this interval was minimal (0.027 ms). A decrease in I production by 5% to 30% was recorded only when this interval reached 1.45 ms. The lower I yield for this case may be explained by the effect of loss reactions (F-3), (F-4), and F-6) that competed with the production reaction (F-2).

The effect of the time interval between the HI injection and atomic I detection is illustrated in **Fig. 31** for different HI flow rates at constant F_2 and NO flow rates. It can be seen that the rate of I production was lower by 35% to 50% when this time interval was increased from 2.1 ms (curves 1) to 2.7 ms (curves 2). The atomic I flow rates measured in the second detection cell (corresponding to a time interval of 9.4 – 10 ms) were several times lower. This result reflects the important effect of I atom loss reactions, mainly by reactions (F-10)-(F-12).

2.4. Results obtained with the transverse flow reactor

2.4.1. Conditions for measurements of atomic I concentration profile along the gas flow

The experimental configuration with the reactor 2 shown in Fig. 27 made possible to shorten a distance between injection of the last reactant (HI or NO) and the nearest position of movable ISD probe beam up to 12 mm. This nearest probe position is designated in figures as a relative position 0 mm, and corresponds to a time interval of 0.45 ms between injection of the last reactant and I detection. The most distant position of the probe beam along the flow was 48 mm corresponding to a time interval of 2 ms.

In one set of measurements, the NO/ N_2 mixture was injected into the primary flow of F_2/N_2 mixture through the injector placed in the cavity center and the HI/ N_2 mixture through two injectors embedded in the walls (this order of injectors is designated below as NO-HI). In further set of experiments, the NO and HI gases were injected in a reverse order (the order of injectors HI-NO). Concentration profiles of atomic I concentration along the gas flow were recorded in the investigated region at constant flow rate of all reagents. The probe beam moved in the duct axis with a speed of 4 mm/s. During the first experiments, the probe was moved downstream and upstream along the gas flow through the investigated region. Because it had no effect on measured values of I concentration, the next records were performed in one direction only.

2.4.2. Measurements with the injectors order NO-HI

Fig. 32 illustrates the profiles of atomic I flow rate along the gas flow for three values of F_2 flow rates at constant NO and HI flows. Twofold I production was measured when F_2 flow rate was 2.7 times higher, which follows from comparison of curves 1 and 2. With further increase in F_2 flow rate (curve 3) the I flow rate was similar like in the curve 2, but only at the beginning of the optical cell, and then declined along the gas flow. It was ascribed to a detrimental effect of the reaction $I + F_2$ (F-12). When HI flow rate was higher (300 $\mu\text{mol/s}$) at similar F_2 flow rate, no

declining I concentration was observed, which was explained by I formation from excessive HI molecules and F atoms generated in the reaction (F-12).

Fig. 33 shows an example of results obtained with different NO flow rates, X, to other reactants, i.e. $F_2 : NO : HI = 1 : X : 0.82$, where $X = 0.65, 1.1, 1.9, 2.3$, and 3, respectively. No substantial effect of NO flow rate on atomic I production was found for X between 1.1 and 2.3, only a slight decline of I concentration along the gas flow was observed. It was rather surprising that I production rate was not lower even if the NO/F_2 ratio = 0.65. A little lower I production rate (curve 5) at a great excess of NO over F_2 could be ascribed to loss reactions (F-3) and (F-4). A substantially lower rate of I production (about 2x) was observed only at $NO/F_2 = 0.25$, where a significant NO deficit limited the rate of reaction (F-1).

An example of the effect of HI flow rate on the I production rate is shown in **Fig. 34**. A low HI flow rate in relation to F_2 and NO flow rates resulted in a lower I production which was caused by deceleration of the production reaction (F-2) (see curves 1, 2).

This study showed that rather effective and steady production of atomic iodine was achieved when the reacting gases were approximately in the equimolar ratio. This is in accordance with the stoichiometry of the reactions (F-1) and (F-2). A significant deficit of F_2 or NO limited the rate of reaction (F-1), and insufficient HI flow rate limited the rate of reaction (F-2). An excess of F_2 over NO at simultaneous lack of HI was detrimental due to acceleration of I loss-reaction (F-12). The NO/F_2 ratio could attain even 2.3 without a negative effect on the rate of I production. A sufficient production of atomic I was achieved also at a moderately lower flow rate of HI vs. F_2 or NO, which is demonstrated by curves 3 and 4 in **Fig. 35**. In this experiment, the I concentration decreased only from $3 \times 10^{15} \text{ cm}^{-3}$ to $2.4 \times 10^{15} \text{ cm}^{-3}$ in the time interval between 0.45 and 2 ms from HI injection. A substantial excess of HI vs. stoichiometry did not enhance I production significantly, e.g. an increase in the HI/F_2 ratio (or HI/NO ratio) from 1.22 to 2.6 increased I production rate 1.18times only (see curves 4 and 3 in Fig. 34).

2.4.3. Measurements with the injectors order HI-NO

The reverse order of HI and NO injection into the primary flow with F_2 was examined with the aim to reduce the effect of the loss-reactions (F-3) and (F-4) that compete the atomic I production reaction (F-2). This was supported by the modeling results, by which the rate of reaction (F-2) is limited by the mass-transfer rate of generated F atoms to HI jets. The F atoms formed at the interface of primary gas flow and NO jets, however, could react with NO molecules rather fast (F-3) due to their high local concentration and their high diffusion

coefficient (approximately twice higher than HI molecules). In case of the NO-HI injection order the HI molecules are therefore worse available for the reaction with F atoms. It was presupposed that the HI-NO injection order could create a more uniform mixture of HI with F₂ before the NO injection, and a loss of F atoms via the reactions (F-3) and (F-4) could be thus lower. An example of the results is shown in **Fig. 36**. The maximum of I production rate was shifted with increasing F₂ flow rate in the upstream direction which reflects an acceleration of both production and loss reactions. The production of I atoms was nearly twice higher than in the case of NO-HI injection order at comparable flow rates of reacting gases. This is obvious from a comparison of curves 1 and 2 in Fig. 36 with the curve 2 in Fig. 32, or the curve 4 in Fig. 33. The yield of atomic iodine was about 60 % (related to HI) for the NO-HI injectors order. This proved our assumption of better HI utilization for this injection order.

2.4.4. Temperature of the reaction mixture

Temperature of the reaction mixture was measured by a thermocouple (see Fig. 27) and also evaluated from the shape of absorption-frequency (or emission-frequency) curves obtained by the ISD measurements. The first method suffered from a rather long time response of the thermocouple, which was ~ 40 s for a temperature drop by 40 K. The calculated values from the ISD measurements were rather scattered with the standard deviation typically of 50 K. Nevertheless, the temperature data from both methods were in a quite good agreement. This is evident from **Fig. 37** where the temperature was evaluated for two F₂ flow rates from the ISD data represented by curves 1 and 2 in Fig. 32 (open points), and measured by the thermocouple (full points). The measured temperatures ranged between 320 and 500 K, and increased mostly by increasing the F₂ flow rate. It is illustrated in **Tab. 2** where the gas temperature was obtained by the thermocouple in measurements corresponding with data in Fig. 32.

Tab. 2

Effect of F₂ flow on gas temperature: $n_{\text{NO}} = 221 \mu\text{mol s}^{-1}$, $n_{\text{HI}} = 134 \mu\text{mol s}^{-1}$

$n_{\text{F}_2}, \mu\text{mol s}^{-1}$	58	159	277
T, K	333	397	432

The temperature increase can be ascribed to increasing rates of exothermic reactions F₂ + NO (F-1), F + HI (F-2), and F₂ + I (F-12). The highest gas temperature was recorded for extremely high F₂ flow rate, which is evident from **Tab. 3**.

Tab. 3Effect of F₂ flow on gas temperature: $n_{\text{NO}} = 65 \mu\text{mol s}^{-1}$, $n_{\text{HI}} = 295 \mu\text{mol s}^{-1}$

$n_{\text{F}_2}, \mu\text{mol s}^{-1}$	40	260	600
T, K	328	430	505

A significant increase in temperature with increasing F₂ flow rate in the range of $n_{\text{F}_2}/n_{\text{NO}} \gg 1$ was rather surprising. This phenomenon could be caused by a strongly exothermic reaction (F-14). As the rate constant of this reaction was not found in the literature, we performed some measurements for its approximate estimation. The experimental arrangement is described in chapter 2.2. The measurement was performed at $100 - 320 \mu\text{mol s}^{-1}$ F₂ + $100 \mu\text{mol s}^{-1}$ HI. The rate constant of reaction (F-14) was calculated both from 488 nm light absorption and from the measured temperature increase of the reaction mixture. Both methods resulted in the rate constant $k_{14} \leq 1 \times 10^{-15} \text{ cm}^3 \text{ s}^{-1}$ that is too low to confirm the explanation given above.

An increase in NO flow had the opposite effect on the gas temperature, which is documented in **Tab. 4**. These data concern the measurements presented in Fig. 33.

Tab. 4Effect of NO flow on gas temperature: $n_{\text{F}_2} = 159 \mu\text{mol s}^{-1}$, $n_{\text{HI}} = 130 \mu\text{mol s}^{-1}$

$n_{\text{NO}}, \mu\text{mol s}^{-1}$	104	172	306	371	486
T, K	420	412	398	397	392

The observed temperature decrease with increasing NO flow rate even in the region of the ratio $\text{NO}/\text{F}_2 < 1$ seems to be in contradiction with the first order of the reaction (F-1). A slight decrease in temperature at an excess of NO can be ascribed to a cooling effect of the excessive NO/N₂ mixture.

An increasing production of atomic I with increasing HI flow (see Fig. 34) at the ratio $\text{HI}/\text{F}_2 < 1$ was accompanied with a slight temperature increase (see **Tab. 5**), which can be explained by higher rate of the exothermic reaction (F-2). An excessive HI+N₂ mixture (at $\text{HI}/\text{F}_2 > 1$) had probably the same “cooling” effect as the excessive NO+N₂ mixture.

Tab. 5Effect of HI flow on gas temperature: $n_{\text{F}_2} = 186 \mu\text{mol s}^{-1}$, $n_{\text{NO}} = 181 \mu\text{mol s}^{-1}$

$n_{\text{HI}}, \mu\text{mol s}^{-1}$	61	128	225	472
T, K	401	429	427	417

2.5. Conclusions from this investigation

The experimental investigation of chemical generation of atomic iodine for a COIL via atomic fluorine was performed at the total pressure in the range of 1 and 2.5 kPa. The reacting gases (F_2 , NO and HI) were used in 10 % mixtures with nitrogen. The effective and rather steady production was achieved at the NO : F_2 ratio ranged from 0.8 to 2.3. When F_2 flow rate was too low, the intermediate F atoms were produced with rather low rate in the reaction $F_2 + NO$. This limits also the rate of atomic iodine generation. An excessive F_2 at a simultaneous lack of HI substantially increases a loss of atomic iodine in the reaction with F_2 , while this reaction has no negative effect when the HI flow rate is sufficiently high. The formed F atoms can then further react with HI to atomic iodine. A low NO flow rate caused a low production of atomic iodine due to a limited rate of its reaction with F_2 to form F atoms. A considerable excess of NO decreased the F production (and consequently also I) only slightly. A too low flow rate of HI limited the rate of its reaction with F, and the excessive HI had no substantial negative effect on I production.

The atomic iodine production was affected significantly by the order of secondary gases (NO and HI) injection. Nearly twice higher rate of I production was recorded with the HI injection first and the NO injection next. This was explained by a better utilization of HI in reaction with formed atomic fluorine.

The temperature of the reaction mixture ranged between 320 K and 500 K. It increased mainly with increasing F_2 flow rate due to the exothermic reaction with NO. An excessive NO and/or HI flows caused a lowering the temperature by a cooling effect. A reason of the observed temperature increase on increasing F_2 flow rate (at F_2 excess) was not explained yet.

The investigated method of chemical generation of atomic iodine via F atoms provided rather steady concentrations of atomic iodine. The highest concentration obtained from the presented results was $3 \times 10^{15} \text{ cm}^{-3}$ within the time interval of 0.45 to 2 ms after admixing of the last reactant (HI or NO). This concentration should be sufficient for operation of the supersonic COIL.

We performed recently measurements of atomic I production at higher flow rates of reacting gases, that is why at higher pressures in the reactor (3 – 8 kPa), and temperatures (500 – 600 K). This resulted in higher I concentrations (do $5 \times 10^{15} \text{ cm}^{-3}$) in comparison with the values given above, but the yields of atomic iodine related to the flow rates of reacting gases were lower. These results will be contained in the interim report of the next grant in February 2004.

The experimental results and modeling results showed that the yield of produced I atoms decreases with increasing total pressure, which is caused by the increase in the rate of termolecular loss-processes with pressure including atomic F (F-3), (F-4), and (F-6), and also atomic iodine (F-7) - (F-10), in the contrary to the rate of bimolecular reactions for F and I atoms production. A low-pressure generation of atomic fluorine (at 1 – 2.5 kPa) by this way is disadvantageous because the reaction time is very long (0.5 – 1 ms in given conditions). This corresponds to a reaction path of 10 – 20 cm in the gas channel upstream the supersonic nozzle. This would result in a significant losses of I^* on a such long reaction path and in the primary stream containing $O_2(^1\Delta)$ and water vapor. It would be therefore more advantageous to generate atomic fluorine in a separate reactor, and inject them into $O_2(^1\Delta)$ stream together with HI closely the nozzle. This would be limited by pressure in the reactor that must be higher then pressure in the injection place in the COIL.

The second possible way is the generation of atomic F at high temperatures (above 1000 K). It would require using rather concentrated gases (F_2 , NO) to attain needed temperature. By a preliminary calculations, the temperature of 1100 K and about 50 % conversion of F_2 to F would be possible to attain using the concentrated NO and 20 % F_2 . More detailed calculations and experiments will be contained in the next EOARD report.

3. Progress in mathematical modeling

3.1. Introductory remarks

In conventional COIL systems, molecular iodine vapor is injected from the walls to the gas stream containing $O_2(^1\Delta)$. The diffusion flux of I_2 into the primary stream is much smaller then the reverse diffusion flux of $O_2(^1\Delta)$ into the I_2 jet due to a large excess of $O_2(^1\Delta)$ over I_2 and smaller $O_2(^1\Delta)$ molecular weight (see **Tab. 6**). The mixing plane thus occur in the vicinity of the jet axis. The COIL with an instantaneous chemical generation of atomic iodine in flowing laser medium brings a completely new situation. The chemical kinetics of the atomic iodine generation, as well as the coupling between chemistry, mass transfer and fluid dynamics, differs substantially from the COIL with molecular iodine. The reactants contained in the primary gas (ClO_2 and then Cl) are diluted and diffusion occurs predominantly from the jet to its surroundings (**Tab. 6**).

Tab.6

Diffusion fluxes and second Damköhler numbers for different gas-to-gas penetration

secondary gas	direction	flux ($\mu\text{mol}/\text{cm}^2/\text{s}$)	Da_{II} (orders of mag)
I_2 (He)	I_2 jet \rightarrow primary flow	0,264	1
	$\text{O}_2(\Delta)$ prim.fl. \rightarrow jet	321	
NO (N_2)	NO jet \rightarrow prim.fl.	2,38	10^2
	ClO_2 prim.fl. \rightarrow jet	0,032	
ClO_2 (N_2)	ClO_2 jet \rightarrow prim.fl.	0,77	10^2
	NO prim.fl. \rightarrow jet	0,0954	
HI (N_2)	HI jet \rightarrow prim.fl.	0,705	10^4
	Cl prim.fl. \rightarrow jet	0,0043	

Besides, the second Damköhler number relevant to I_2 dissociation is of the order of unity, while the same numbers relevant to atomic chlorine and atomic iodine generation are $\text{Da}_{\text{II}} \approx 10^2$ and $\text{Da}_{\text{II}} \approx 10^4$, respectively. This means that diffusion is the rate-controlling process and must be therefore carefully handled. This fact would demand to formulate exactly the multicomponent molecular diffusion (the Stefan-Maxwell equations). However, thanks to a large excess of buffer gas and small differences between diffusion coefficients of the species, a general formulation of the Fick's law dilute approximation will probably not cause a significant error.

The fast reaction chemistry implicates that atomic chlorine, and subsequently atomic iodine, appears very close to a mixing point of the reacting gases and the concentration field is thus very sensitive to a distance between NO and HI injectors and to penetration depths of both gases.

The three-dimensional (3-D) computational fluid dynamics (CFD) models were developed to understand in more details the processes that occur after injecting the reactants (ClO_2 , NO, HI) into the primary gas stream in COIL. Initially, a simplified model was developed including only the interaction between a single NO jet and the primary flow in the subsonic part of the laser. The physical domain was extended in the second step to two-rows-orifice injection of NO and HI into the primary flow of ClO_2 in helium. Further, the modeled flow channel was extended to include the supersonic nozzle.

3.2. Modeling of atomic chlorine generation in the COIL subsonic channel

The previous 1-D modeling [17] showed that the reaction between NO and ClO_2 runs through different mechanisms depending on the flow rate ratio of reactants. Radical ClO was the main product for the ratio of NO : $\text{ClO}_2 = 1 : 1$. If NO gas is in excess (e.g., NO : $\text{ClO}_2 = 2 : 1$), Cl atom and ClO radical act as chain carriers, and higher yields of Cl atoms are produced within a shorter reaction time. This behavior must be, however, revised with the aid of 3-D modeling because the reaction mechanism is influenced by the finite mixing.

A character of the flow (laminar or turbulent) for the case of a jet in a cross flow is related to the momentum flux ratio between the secondary jet and the primary flow, described by the relation

$$q = (\rho u^2)_{jet} / (\rho u^2)_{prim}, \quad (\text{M-1})$$

where ρ and u are density and velocity of the jet (at the orifice place) and primary flow, respectively. At the low momentum ratio, the level of turbulence initially present in the primary flow controls the downstream mixing. For the COIL conditions, this flow is predominantly laminar ($\text{Re} \approx 10^4$). Maximum turbulence intensity is $\sim 10\%$ for q values of 10-15 typical for the subsonic channel of our COIL, and at a distance of 20 orifice diameters downstream from injection. Only one model of turbulence - the large eddy simulation (LES) - was shortly tested here and compared with the laminar solution.

3.2.1. Description of the model

The computational domain was derived from the mixing nozzle of the experimental device, whose schematic diagram is shown in **Fig. 37**. The origin of coordinate system was placed in the

orifice center. The x-axis was in the flow direction, the y-axis was the lateral direction and the z-axis was parallel to the orifice axis. The NO gas was injected 14 mm upstream the supersonic nozzle throat. The rectangular subsonic channel for the primary gas was 10 mm high and 50 mm wide. A symmetry was applied in computations, i.e. the region from the center of the orifice to the midpoint between neighboring orifices, and a half of the channel height was modeled only. The 3-D Navier-Stokes equations coupled to the finite rate chemistry were solved by the finite-volume method using the commercial code Fluent made by Fluent Inc. The computational domain was divided into 268010 hexahedral cells. The inlet boundaries kept the fixed mass flow rates and the gas temperature of 300 K. The outlet boundary was kept at the constant outlet pressure of 3 kPa, which was taken from the experimental pressure recording 3 cm upstream of the nozzle throat. A non-slip walls with constant temperature (300 K) were considered. The NO gas was diluted by nitrogen in the ratio 1 : 9. The primary flow contained oxygen (non-reactive ground state), helium, nitrogen (used for ClO₂ dilution), and a small amount of chlorine (coming from the SOG). Chemical reactions incorporated into the model and their rate constants are listed in **Table 7**

Tab. 7
A finite rate chemistry model (see Ref. 17 and 18)

$\text{ClO}_2 + \text{NO} \rightarrow \text{ClO} + \text{NO}_2$	(M-2)	$2.51 \times 10^{-12} \exp(-4989/8.314/T)$
$\text{ClO} + \text{NO} \rightarrow \text{Cl} + \text{NO}_2$	(M-3)	$6.39 \times 10^{-12} \exp(2411/8.314/T)$
$\text{Cl} + \text{ClO}_2 \rightarrow 2 \text{ClO}$	(M-4)	$3.40 \times 10^{-11} \exp(1330/8.314/T)$
$\text{Cl} + \text{NO}_2 + \text{M} \rightarrow \text{NO}_2\text{Cl} + \text{M}, \quad \text{M} = \text{N}_2, \text{O}_2$	(M-5)	$1.3 \times 10^{-30} (T/298)^{-2}$
$\text{Cl} + \text{NO}_2 + \text{M} \rightarrow \text{NO}_2\text{Cl} + \text{M}, \quad \text{M} = \text{He}$	(M-6)	1.8×10^{-31}
$\text{ClO} + \text{NO}_2 + \text{M} \rightarrow \text{NO}_3\text{Cl} + \text{M}, \quad \text{M} = \text{N}_2, \text{O}_2$	(M-7)	$3.69 \times 10^{-33} \exp(9562/8.314/T)$
$\text{ClO} + \text{NO}_2 + \text{M} \rightarrow \text{NO}_3\text{Cl} + \text{M}, \quad \text{M} = \text{He}$	(M-8)	$2.78 \times 10^{-33} \exp(9030/8.314/T)$
$\text{Cl} + \text{NO}_2\text{Cl} \rightarrow \text{Cl}_2 + \text{NO}_2$	(M-9)	5.5×10^{-12}
$\text{Cl} + \text{NOCl} \rightarrow \text{Cl}_2 + \text{NO}$	(M-10)	$6.59 \times 10^{-11} \exp(-1054/8.314/T)$
$\text{Cl} + \text{Cl} + \text{M} \rightarrow \text{Cl}_2 + \text{M}, \quad \text{M} = \text{N}_2, \text{O}_2$	(M-11)	$1.6 \times 10^{-33} \exp(6693/8.314/T)$
$\text{Cl} + \text{Cl} + \text{M} \rightarrow \text{Cl}_2 + \text{M}, \quad \text{M} = \text{He}$	(M-12)	$4.05 \times 10^{-33} \exp(1081/8.314/T)$

The thermodynamic and transport data were taken from the NIST Chemistry Webbook [19] and Ref. [20]. For simplicity, the heat capacity and viscosity data were kept constant at 300 K, except for nitrogen and helium buffer gas, for which the temperature dependence was based on the polynomial fit of the published data. The mixture properties were calculated using the ideal gas mixing law or mass-weighted mixing law. The binary diffusion coefficients were calculated using the kinetic theory from the Lennard-Jones parameters of pure gases.

3.2.2. Modeling results

3.3.2.1. Model case 1: the cold flow and low NO flow rate

In the first simulation, a non-reactive case was considered with laminar and LES formulation, respectively, to calculate the mixing of NO with primary gas. Molecular diffusion was modeled first by the Fick's law dilute approximation. The molar flow rates of pure gases are listed in **Table 8**.

For the purpose of this simulation, an underpenetrated case was considered with flow rates ratio NO : ClO₂ = 0.58 : 1 to obtain the information about mixing both up and down the jet axis.

Tab. 8
Total molar flow rates of pure gases for all model cases.

molar flow rate, mmol s ⁻¹	Model case 1 and 2	Model case 3 and 4
ClO ₂	1.825	1.825
Cl ₂	0.744	0.744
primary N ₂	6.954	6.954
primary He	69.5	69.5
primary O ₂	33.01	33.01
NO	1.063	3.666
secondary N ₂	9.571	32.99

The simulation results on penetration of the secondary jet into the primary stream were compared with three empirical equations for the jet trajectory (based on the maximum velocity trajectory) [21], [22]

$$z/D = q^{0.43}(x/D)^{0.33}, \quad (\text{M-13})$$

$$z/D = (qx/D)^{0.394}, \quad (\text{M-14})$$

$$z/D = 0.89q^{0.47}(x/D)^{0.36}, \quad (\text{M-15})$$

where D is the orifice diameter. The q value for the simulated case was calculated *a priori* from the definition (M-1) in the following manner: the primary properties were calculated from the measured pressure, temperature and total molar flow rate using the ideal gas law

$$\rho = pW/RT, \quad (\text{M-16})$$

$$u = nRT/pA, \quad (\text{M-17})$$

where W and n are the molecular weight and molar flow rate of the primary flow, respectively, and A is the cross-section of the flow channel. The secondary gas pressure and temperature were calculated from the total pressure and temperature of the secondary flow using the ideal-gas isentropic equations for the Mach number $M = 1$ because the orifice was designed for the sonic flow. The total pressure was calculated from the molar flow rate through the orifice using the equation for the sonic orifice

$$n = c_d p_s A_s \sqrt{\frac{\kappa R T_s}{W_s} \left(\frac{2}{\kappa + 1} \right)^{\frac{\kappa + 1}{\kappa - 1}}}, \quad (\text{M-18})$$

where p_s and T_s are the total secondary gas pressure and temperature, W_s and κ are the molecular weight and adiabatic constant of the secondary flow, respectively, and A_s is the orifice cross section. The value for the discharge coefficient $c_d = 0.67$ for the circular orifice with sharp edges was taken from the chemical-engineering tables.

A jet axis trajectory for the present simulation is shown in **Fig. 38**. The results of laminar and LES model were nearly identical, only a small difference appeared further downstream. The agreement between simulated and empirical results was very good for all three equations up to $x = 5.7$. For larger x , the simulated results deviated, yielding a smaller penetration. This fact could be explained by the effect of opposite jet (the empirical equations were derived for a single jet in the cross flow of the large height). Fig. 38 shows also the trajectory of the maximum NO concentration, which reached approximately 70% of the velocity trajectory depth. This observation is consistent with the measurement of Cohen *et al.* [23], who correlated the penetration heights and concentration profiles for the injection of He, Ar and Freon-12 into the air stream. The yz contours of NO concentration at different downstream distances are shown in **Fig. 39**. Due to underpenetration, the concentration of NO was still strongly inhomogeneous in the z -direction at $x = 13$ mm from the orifice, although the mixing in the $+z$ direction from the maximum was quite good. The contours have the typical horseshoe-like shape, which vanishes at $x = 13$ mm, as the mixing proceeds in y -direction. The LES results for NO concentration are nearly indistinguishable from the laminar results in this distance range of and therefore they are not shown here.

3.2.2.2. Model case 2: the reactive flow and low NO flow rate

The penetration depth of the NO jet was evaluated in the same way like in the Model case 1, and no difference was found from the non-reactive case. This fact is consistent with the

experimental study of Kamotanyi *et al.* [21] The contours of Cl concentration in several yz planes, and xz, $y = 0$ plane, respectively, are shown in **Figs. 40 a,b**. The maximum Cl concentration corresponded with the maximum NO concentration in the non-reaction case. The anisotropy in Cl concentration is, however, greater than for the NO concentration because of the effect of loss processes.

To assess the effect of molecular diffusion, a comparative simulation was performed with the same parameters, only the Fick's law was replaced by the Stefan–Maxwell equations. The Cl concentration seemed to be the most sensitive quantity. The z-profiles of this concentration (at $y=0$) for both diffusion models are shown in **Fig. 41**. The difference between both results is apparent, but not significant in the global scale. The CPU time required for one iteration with the Stefan-Maxwell solution was by about 30% longer than for one iteration with the Fick's law. This additional time was consumed for calculation of determinant of the multicomponent diffusion coefficient [24], which required $\mathcal{O}(N^3)$ operations. The present model included 11 species, while the reactive simulation of small signal gain will include 22 species at least. Therefore, the Stefan-Maxwell formulation should be replaced by a simplified model, e.g. by the effective binary diffusion model [25] requiring $\mathcal{O}(N^2)$ operations only.

3.2.2.3. Model case 3: the non-reactive flow and excess of NO flow

In this simulation, the flow rates ratio $\text{NO} : \text{ClO}_2 = 2 : 1$ was chosen to observe the mixing behavior of the deeply penetrated NO jet. The penetration depths and depths of maximum NO concentration are shown in **Fig. 42**. The agreement with the empirical equations was very good again. On the contrary to the low penetration case, the NO concentration maxima are very close to the penetration depths.

3.2.2.4. Model case 4: the reactive flow and excess of NO flow

The contours of Cl concentration in several yz planes, and xz, $y = 0$ plane, respectively, are shown in **Figs. 43 a,b**. In comparison with the low NO flow, Cl is more spread in both y and z direction, which confirms the fact that the mixing is controlled predominantly by molecular diffusion.

The previous premixed 1-D modeling showed that the Cl atom yield critically depended on the $\text{NO} : \text{ClO}_2$ flow rates ratio. The results of this 1-D modeling are shown in **Figs. 44 a,b** together with the simulated cases 2 and 4. In the 1-D model, the Cl maximum concentration was 18 times higher for the case of excessive NO, against the case of deficient NO. On the contrary,

in the 3-D simulation the Cl concentration was only two times higher in the case of excessive NO. This fact can be explained by the diffusive mixing, which slows down the formation of ClO radical. However, it is probably the local excess of NO in the mixing interface that provides a higher yield of Cl than predicted by the 1-D model for the ratio $\text{NO} : \text{ClO}_2 = 0.58$.

A concentration of Cl atoms cannot be directly measured but a concentration of I atoms can be evaluated after the reaction of Cl with HI (titration). The yield of I atoms measured on our device was up to 10 times higher for the flow rate ratio $\text{NO} : \text{ClO}_2 = 2 : 1$ than for $1 : 1$. This does not agree with the results of 3-D modeling concerning the effect of the flow rate ratio on atomic chlorine production. It could be, however, explained by the effect of HI, which consumes chlorine atoms, and influences thus chlorine chain kinetics.

The diffusion-controlled mechanism is manifested also by a slowly increasing concentration of both Cl and ClO with the x-coordinate, and by the fact, that there is no significant difference between the x-coordinates of their maxima. The 3-D results are consistent with the previous 2-D modeling of the same reaction system under similar conditions [26].

3.3. Modeling of chemical generation of atomic iodine

The 3-D CFD modeling of the whole reaction system $\text{ClO}_2/\text{NO}/\text{HI}$ for atomic iodine generation started several months ago. The system was modeled first as a cold flow without chemical reactions to study the mixing only and to get a good starting point for the reactive simulation. The results have not been evaluated completely yet, therefore we present here only the results of penetration depth study, to be able to compare them with the results of ClO_2/NO system given above.

The mathematical model was identical with the model described in the section 3.1.1., the laminar flow was considered, and diffusion was modeled by the Fick's law dilute approximation. The computational domain was extended to cover the whole region drawn in Fig.1, and in the downstream direction up to a position of several centimeters downstream the optical resonator axis. The number of cells approached 2 millions. The flow rates of gases were slightly different from the model case 2, and the primary flow did not contain non-reactive oxygen. Both NO and HI were diluted with N_2 in the ratio $1 : 9$. The flow rates are summarized in **Tab 9**.

Tab. 9
Total molar flow rates of pure gases for the model of $\text{ClO}_2/\text{NO}/\text{HI}$ system

Species	molar flow rate, mmol s^{-1}
---------	---------------------------------------

ClO ₂	1.5
Cl ₂	0.25
primary N ₂	15
primary He	70
NO	2.7
HI	1.4

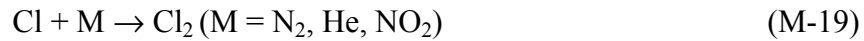
3.3.1 Results of penetration depths

The values of q were calculated in the same manner like in the chapter 3.1.1, separately for NO and HI injectors. The dependence of penetration depths compared with the prediction made by the relation (M-14) is presented in **Figs. 45** and **46** for NO and HI large orifice, respectively. It is apparent that the agreement with the prediction is worse for both gases than with the “single row” injection only in the system ClO₂/NO. It is evident that the jets are not sonic like in the ClO₂/NO system but they are locally supersonic – see **Fig. 47**. This could be one possible explanation of the disagreement between the modeling and the empiric equation.

3.4. 1-D premix modeling of small signal gain in COIL with atomic iodine generation

The values of small signal gain measured on our COIL device with ClO₂/NO/HI system were small in respect to the measured O₂(¹Δ) and the concentration of atomic iodine measured in the system without O₂(¹Δ). We tried to explain this fact by means of a relevant model.

If the modeling of I* - I gain with HI as a precursor is considered, the reaction kinetics of all secondary gases, reaction products and components of primary flow must be known. Among the following main loss processes,



only the reaction (M-21) includes one of the primary flow components.

An impact of the loss processes on the small signal gain may be found by comparing the gain calculated from the chemical kinetics using the premix 1-D model with the maximum available theoretical value calculated using the equilibrium constant of the pumping reaction

$$g_{theor} = 1.3 \times 10^{-16} T^{1/2} 0.5[I] \frac{(1 + 2K)Y - 1}{(K - 1)Y + 1} \quad (M-24)$$

This comparison was performed for conditions typical in our COIL:

Flow rates (mmol s⁻¹): primary: 87 He, 35 Cl₂, 1.3 ClO₂ (in N₂ 1:9)
secondary: 2.7 NO (in N₂ 1:9), 1.4 HI (in N₂ 1:9)
O₂(¹Δ) yield: Y = 0.5
Pressure: subsonic 3.5 kPa, supersonic 300 Pa
Temperature: subsonic 280 K, supersonic 190 K

The theoretical small signal gain was calculated from the atomic iodine concentration measured in the absence of O₂(¹Δ) in the primary flow, and this value was compared with the small signal gain measured in the presence of O₂(¹Δ). Both these experimental conditions (with and without O₂(¹Δ)) were modeled by means of 1-D kinetic model. The theoretical gain was calculated from the modeled atomic iodine concentration as well. Results of calculations and experiments are summarized in **Table 10**.

Tab. 10

experiment	[I] measured without O ₂ (¹ Δ)	ss gain measured with O ₂ (¹ Δ)	theoretical gain from measured [I]	cavity temperature from ISD measurements
	6 x 10 ¹⁴	2.8 x 10 ⁻³	4.5 x 10 ⁻³	190 K
1-D model	[I] calculated without O ₂ (¹ Δ)	ss gain calculated with O ₂ (¹ Δ))	theoretical gain from calculated [I]	cavity temperature (adiabatic)
	6.5 x 10 ¹⁴	5.89 x 10 ⁻³	5.96 x 10 ⁻³	152 K

It can be seen that the model did not agree with measured atomic iodine concentrations. However, the ss gain modeled by the chemical kinetics (with all loss processes) and the gain calculated from the modeled [I] are nearly identical. On the other hand, the theoretical gain calculated from the measured [I] is 1.6 times higher than the measured value. There may be three reasons for this discrepancy:

- 1) some unknown loss processes including either O₂(¹Δ) or I^{*} may exist in the system (a higher experimental temperature could confirm it)
- 2) the production of atomic iodine is slower in presence of the gas flowing from SOG

3) the fluid dynamics or mixing of reactants, which were not included in the simple premixed model, could play a significant role

We plan to prove both these hypotheses in the next work.

Plans for further work on modeling:

Further analysis of the 3-D simulation results of the $\text{ClO}_2/\text{NO}/\text{HI}$ system will first of all study the efficiency of mixing of all three reactive species, and a flow field change after passing the supersonic nozzle. Subsequently, the reactive simulation of this system will be performed.

The 3-D simulation results will be used for developing the quasi-1-D model including finite mixing and fluid dynamics effects. This model will help to prove the hypotheses mentioned in the chapter 3.4.

4. References

- [1] Final report, EOARD contract # SPC 00-4032, Order # F61775-00-WE032, 4 April 2001.
- [2] Final report, EOARD contract # SPC 01-4057, Order # F61775-01-WE057, 10 July 2002.
- [3] Report 001, EOARD contract # SPC 02-4040, Order # FA8655-02-M4040, 16 Jan 2003.
- [4] Report 002, EOARD contract # SPC 01-4057, Order No. F61775-01-WE057, 8 Feb 2002.
- [5] G. Cowley, “*Safety in the design of chlorine dioxide plants*“, Loss Prev. Bull. **113**, 1 (1993).
- [6] Report 001, EOARD contract # SPC 00-4032, Order # F61775-01-WE057, 24 July 2000.
- [7] N.G. Basov, M.V. Zagidullin, V.I. Igoshin, V.A. Katulin, and N.L. Kuprianov, “*Theoretical analysis of the chemical oxygen-iodine lasers*“, Trudy Akademii Nauk SSSR **171**, 30 (1986).
- [8] J.B. Koffend, C.E. Gardner, and R.F. Heidner, “*Photochemistry and kinetics of the $\text{O}_2^* - \text{HI}$ system*“, J. Chem. Phys. **80**, 1861 (1984).
- [9] O. Špalek, V. Jirásek, M. Čenský, J. Kodymová, I. Jakubec, and G.D. Hager, “*Chemical generation of atomic iodine for the chemical oxygen-iodine laser. II. Experimental results*“, Chem. Phys. **282**, 147 (2002).
- [10] J.R. Podolske, H.S. Johnston, “*Rate of the resonant energy-transfer reaction between $\text{O}_2(^1\Delta_g)$ and HOO^\bullet* “, J. Phys. Chem. **87**, 628 (1983).
- [11] J.V. Seeley, R.F. Meads, M.J. Elrod, and M.J. Molina., “*Temperature and pressure dependence of the rate constant for $\text{HO}_2 + \text{NO}$ reaction*“, J. Phys. Chem. **100**, 4026 (1996).
- [12] Y.P. Lee, C.J. Howard, “*Temperature-dependence of the rate-constant and the branching ratio for the reaction $\text{Cl} + \text{HO}_2$* “, J. Chem. Phys. **77**, 756 (1982).

- [13] Report 001, EOARD contract # SPC 01-4057, Order # F61775-01-WE057, 10 October 2001.
- [14] K.M. Gruenewald, J. Handke, F. Duschek, „*Small signal gain and temperature profiles in supersonic COIL*“, Proc. SPIE **4184**, 75-79 (2001).
- [15] G.D. Hager, C.A. Helms, K.A. Truesdell, D. Plummer, J. Erkilli and P. Crowell, “*A simplified analytical model for gain saturation and power extraction in the flowing chemical oxygen-iodine laser*”, IEEE J. Quantum. Electron. **32**, 1525 (1996).
- [16] Report 002, EOARD contract # SPC 02-4040, Order # FA8655-02-M4040, , 16 Sep 2003.
- [17] V. Jirásek, O. Špalek, J. Kodymová, and M. Čenský, „*Chemical generation of atomic iodine for chemical oxygen-iodine laser: Modeling of reaction systems*“ Chem. Phys. **269**, 167 (2001).
- [18] NIST Chemical Kinetics Database, National Institute of Standards and Technology.
- [19] NIST Chemistry Webbook, National Institute of Standards and Technology.
- [20] R. Svehla, NASA Technical Report NASA-TR-R-132 (1962).
- [21] Y. Kamotanyi, I. Greber., AIAA Journal **10 (11)**, 1425 (1972).
- [22] G.N. Abramovich, “*Theory of turbulent jets*“, MIT Press, Boston (1963).
- [23] S.L. Cohen, L.J. Coulter, J.J. Egan, AIAA Journal **9(4)**, 718 (1971).
- [24] Fluent code user’s manual, Fluent. Inc.
- [25] T.J. Madden, W.C. Solomon, AIAA Paper **97-2387** (1997).
- [26] V. Jirásek, O. Špalek, J. Kodymová, and M. Čenský, „*Mixing of gaseous reactants in chemical generation of atomic iodine for COIL: Two-dimensional modeling study*“ Proc. SPIE **5210**, 420 (2002).

5. Acknowledgement

The investigators are very grateful to the USAF EOARD for the financial support of this work, and to Dr. Ingrid Wysong and Dr. Alexander Glass, Program Manager, Lasers and Photonics at the EAORD, for their assistance in the matters concerting this grant.

We thank very much Dr. Gordon Hager from the US AFRL/DE, the contract supervisor, for his encouragement in our work, and beneficial discussions on the contract tasks.

6. Cost Proposal

1. Expendable supplies and materials:		\$9,000
Gases and chemicals, constructional materials	\$6,500	
Optical accessory	\$2,000	
Office, computers and printers supplies	\$500	
2. Travel:		
Within Europe		\$500
3. Publications in Journal, Reports, Literature purchased:		\$500
Preparation of papers and reports	\$200	
Literature purchasing	\$300	
4. Labor-rewards:		\$11,000
Jarmila Kodymová (PI), senior scientist	600 hrs @ \$5,0/hr	
\$3,000		
Otomar Špalek (PI) senior scientist	600 hrs @ \$5,0/hr	
\$3,000		
Vít Jirásek (junior scientist)	600 hrs @ \$3,5/hr	
\$2,100		
Miroslav Čenský (junior scientist)	600 hrs @ \$3,5/hr	
\$2,100		
Jan Kuželka	100 hrs @ \$3,0/hr	
\$300		
1-2 Technicians	200 hrs @ \$2,5/hr	
\$500		
5. Overhead charges to the Institute		\$2,500
Total cost proposal		\$23,500

Principal Investigator

Director of Institute of Physics

STATEMENT


- (1) **The Contractor, Institute of Physics of the Academy of Sciences of the Czech Republic, hereby declares that, to the best of its knowledge and believes, the technical data delivered herewith under Contract No. FA8655-02-M4040 is complete, accurate, and complies with all requirements of the contract.**
- (2) **I certify that there were no subject inventions to declare as defined in FAR 52.227-13, during the performance of the Contract No. FA8655-02-M4040.**

Date: 16 January 2004

Name and Title of Principal Investigator:


Dr. Jarmila Kodymová

Name and Title of Authorized Official:


Ing. Karel Jungwirth, DrSc.
Director of Institute of Physics AS

INSTITUTE OF PHYSICS
Academy of Sciences
of the Czech Republic
182 21 Prague 8, Na Slovance 2
Czech Republic -1-

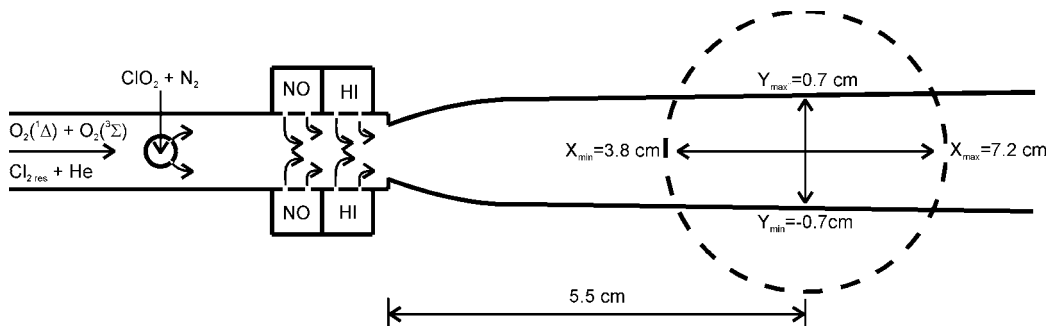


Fig. 1. Cross section of the laser cavity with NO and HI injectors

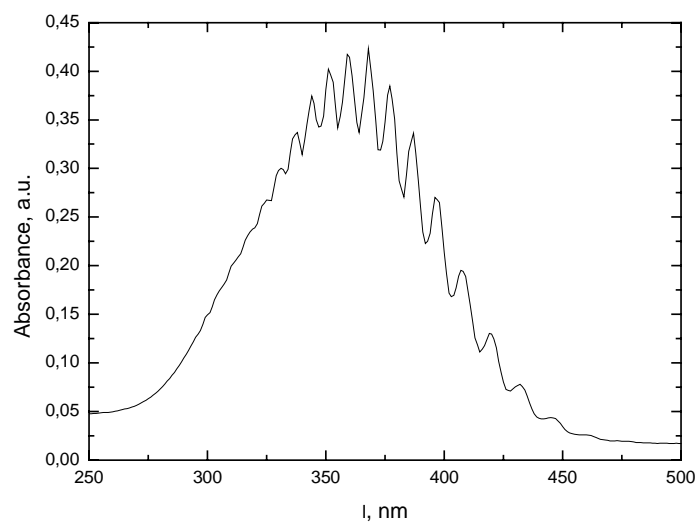


Fig. 2. Absorption curve of ClO_2 measured in the optical cell placed into the gas line between ClO_2 generation and pressure reading probe.

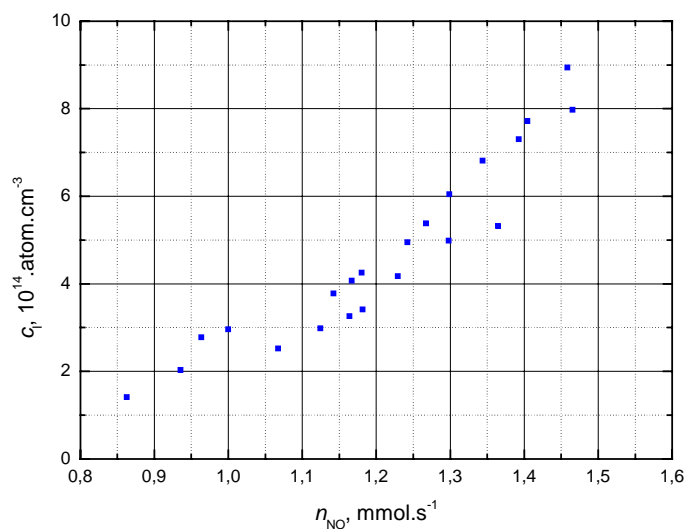


Fig. 3. Effect of NO flow rate on atomic iodine concentration detected in the COIL cavity in flow of non-reactive nitrogen ^{*)}. Primary flow: $0.815 \text{ mmol ClO}_2 \text{ s}^{-1} + 8.2 \text{ mmol N}_2 \text{ s}^{-1}$; 1st injector: 10% NO in N₂; 2nd injector: $0.8 \text{ mmol HI s}^{-1} + 8 \text{ mmol N}_2 \text{ s}^{-1}$.

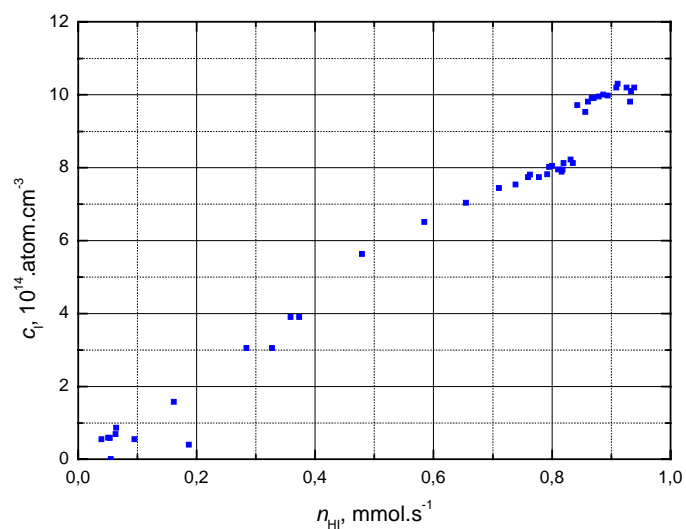


Fig. 4. Effect of HI flow rate on atomic iodine concentration detected in the COIL cavity in flow of non-reactive nitrogen. Primary flow: $0.9 \text{ mmol ClO}_2 \text{ s}^{-1} + 9 \text{ mmol N}_2 \text{ s}^{-1}$; secondary flows: $1.8 \text{ mmol NO s}^{-1} + 16.2 \text{ mmol N}_2 \text{ s}^{-1}$, and 10% HI in N₂.

^{*)} Note: Dependences in Figs. 3 to 5 were measured with the vacuum pump that had about three times lower pumping capacity ($0.278 \text{ m}^3 \text{ s}^{-1}$) than the Roots pump used in further experiments ($0.833 \text{ m}^3 \text{ s}^{-1}$).

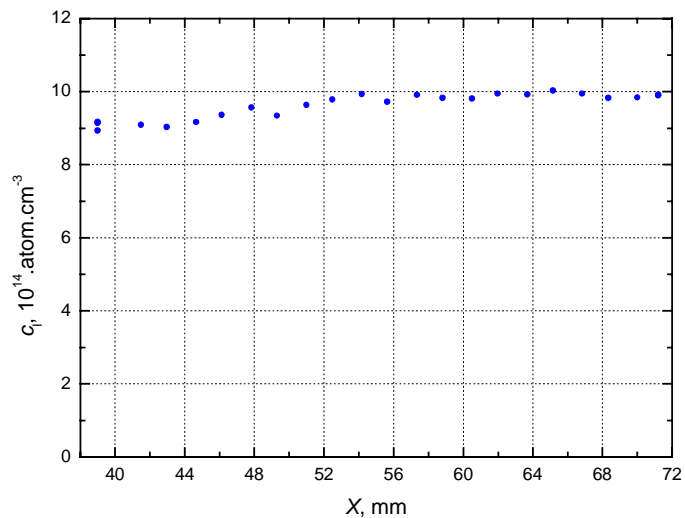


Fig. 5. Concentration of atomic iodine recorded along gas stream through COIL cavity in non-reactive nitrogen, x - distance from the nozzle throat.
 Primary flow: $0.9 \text{ mmol ClO}_2 \text{ s}^{-1} + 9 \text{ mmol N}_2 \text{ s}^{-1}$; secondary flows:
 $1.75 \text{ mmol NO s}^{-1} + 16 \text{ mmol N}_2 \text{ s}^{-1}$, and $0.8 \text{ mmol HI s}^{-1} + 7 \text{ mmol N}_2 \text{ s}^{-1}$.

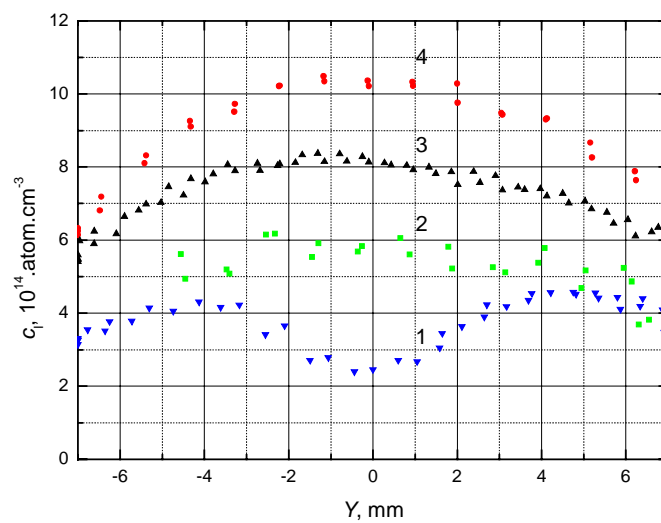


Fig. 6. Atomic iodine concentration profiles across the COIL cavity in non-reactive nitrogen flow recorded for different flow rates of reactive gases.
 Primary flow (all in mmol s^{-1}) $80 \text{ He} + x \text{ ClO}_2$, $n_{\text{ClO}_2} + n_{\text{NO}} + n_{\text{HI}} + n_{\text{N}_2}$: $0.9 + 1.6 + 0.75 + 31$ (curve 1); $1.33 + 2.75 + 1.25 + 50$ (curve 2); $1.8 + 3.05 + 1.5 + 60$ (curve 3); $2.3 + 4.9 + 2.5 + 92$ (curve 4).

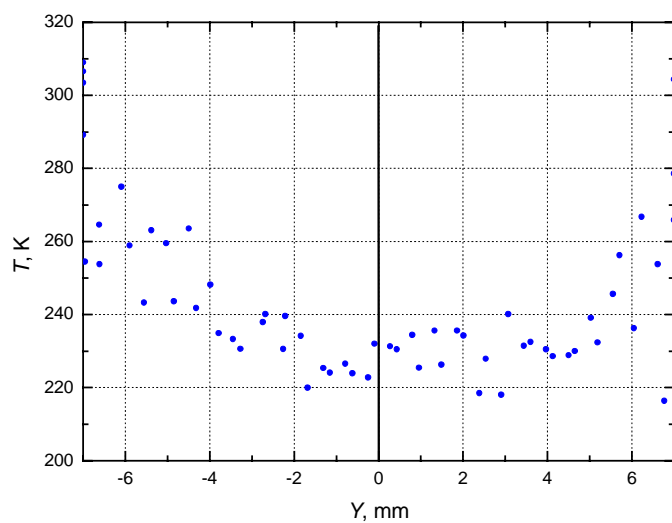


Fig. 7. Gas temperature profile across the cavity recorded for experimental conditions corresponding curve 3 in Fig. 5.

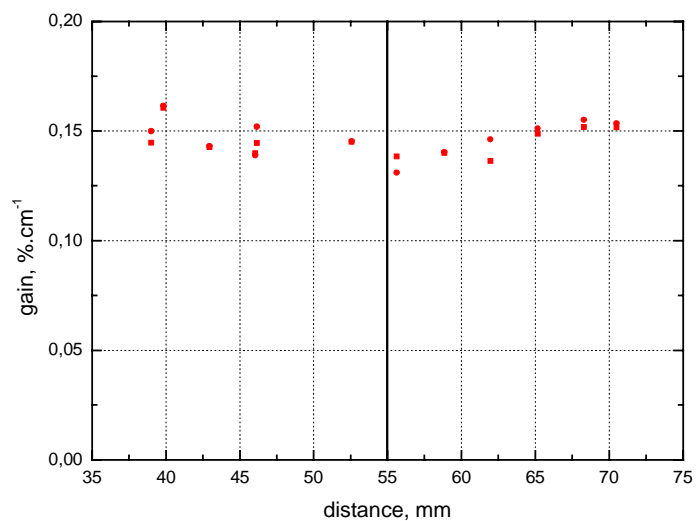


Fig. 8. Gain of atomic iodine recorded in $\text{O}_2(^1\Delta)$ stream along COIL cavity 4 mm above cavity center. Primary flow: $15 \text{ mmol O}_2(^1\Delta) \text{ s}^{-1} + 9 \text{ mmol O}_2(^3\Sigma) \text{ s}^{-1} + 80 \text{ mmol He}_{\text{prim}} \text{ s}^{-1} + 3 \text{ mmol Cl}_{2 \text{ resid}} \text{ s}^{-1} + 0.9 \text{ mmol ClO}_2 \text{ s}^{-1} + 9 \text{ mmol N}_2 \text{ s}^{-1}$; secondary flows: $1.75 \text{ mmol NO s}^{-1} + 9 \text{ mmol N}_2 \text{ s}^{-1}$, and $0.8 \text{ mmol HI s}^{-1} + 8 \text{ mmol N}_2 \text{ s}^{-1}$.

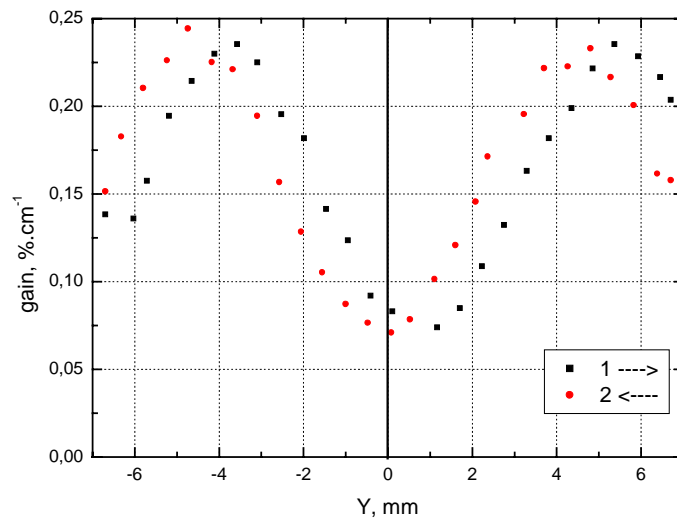


Fig. 9. Gain distribution across the COIL cavity in $O_2(^1\Delta_g)$ flow.
 Primary flow: $80 \text{ mmol He s}^{-1} + 15 \text{ mmol } O_2(^1\Delta) \text{ s}^{-1} + 9 \text{ mmol } O_2(^3\Sigma) \text{ s}^{-1} + 3 \text{ mmol Cl}_2 \text{ s}^{-1} + 1.33 \text{ mmol ClO}_2 \text{ s}^{-1} + 13 \text{ mmol N}_2 \text{ s}^{-1}$;
 secondary flows: $2.7 \text{ mmol NO s}^{-1} + 25 \text{ mmol N}_2 \text{ s}^{-1}$, and $1.25 \text{ mmol HI s}^{-1} + 12.5 \text{ mmol N}_2 \text{ s}^{-1}$.

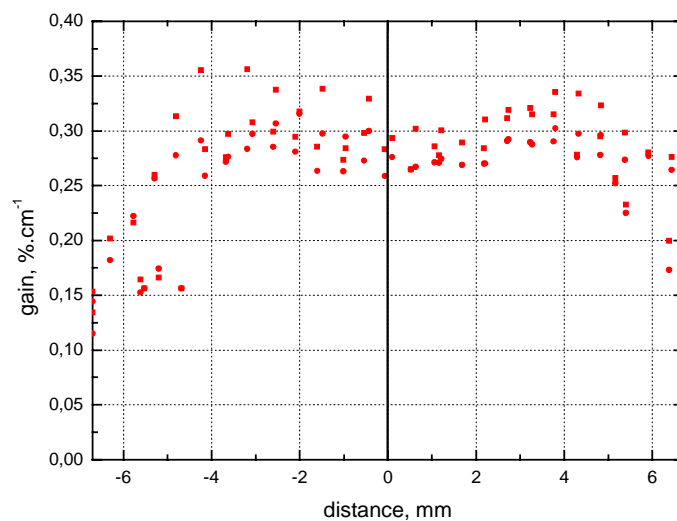


Fig. 10. Gain distribution across the COIL cavity in $O_2(^1\Delta_g)$ flow at higher flow rates of secondary gases. Primary flow: the same as in Fig. 9;
 secondary flows: $4.2 \text{ mmol NO s}^{-1} + 38 \text{ mmol N}_2 \text{ s}^{-1}$, and $2 \text{ mmol HI s}^{-1} + 20 \text{ mmol N}_2 \text{ s}^{-1}$.

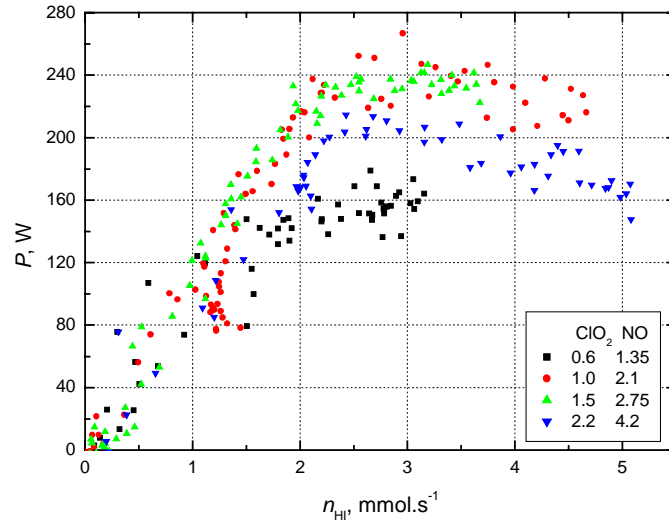


Fig. 11. Laser power in dependence on HI flow at different flow rate of ClO_2 ($\text{NO}:\text{ClO}_2 \approx 2$). Primary gases: $80 \text{ mmol He s}^{-1} + 24 \text{ mmol O}_2 \text{ s}^{-1} + 3 \text{ mmol Cl}_2 \text{ s}^{-1}$; curve 1: $n_{\text{ClO}_2} + n_{\text{NO}} + n_{\text{N}_2} = 0.62 + 1.35 + 18 [\text{mmol s}^{-1}]$; curve 2: $1.0 + 2.1 + 29 [\text{mmol s}^{-1}]$; curve 3: $1.5 + 2.75 + 40 [\text{mmol s}^{-1}]$; curve 4: $2.2 + 4.2 + 47 [\text{mmol s}^{-1}]$; secondary gases: 10 % NO in N_2 , and 10% HI in N_2 .

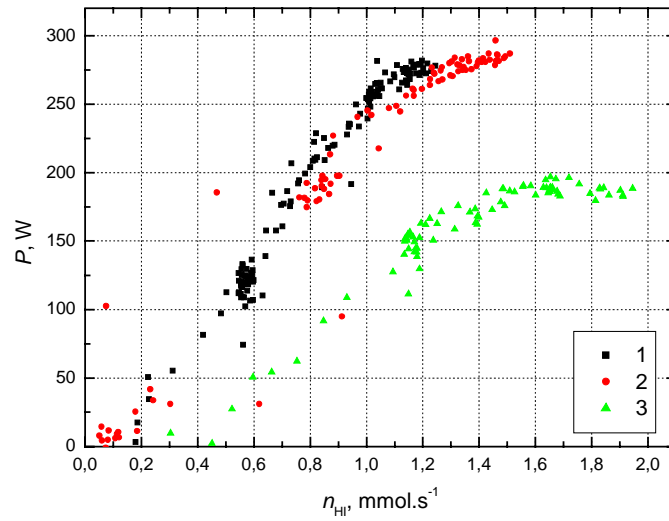


Fig.12. Laser power in dependence on HI flow rate using more diluted HI (5% instead of 10%). Primary flow: $80 \text{ mmol He s}^{-1} + 24 \text{ mmol O}_2 \text{ s}^{-1} + 3 \text{ mmol Cl}_2 \text{ s}^{-1}$; $1.5 \text{ mmol ClO}_2 \text{ s}^{-1} + 15 \text{ mmol N}_2 \text{ s}^{-1}$; secondary flows: $2.7 \text{ mmol NO s}^{-1} + 25 \text{ mmol N}_2 \text{ s}^{-1}$, and 5% HI in N_2 .

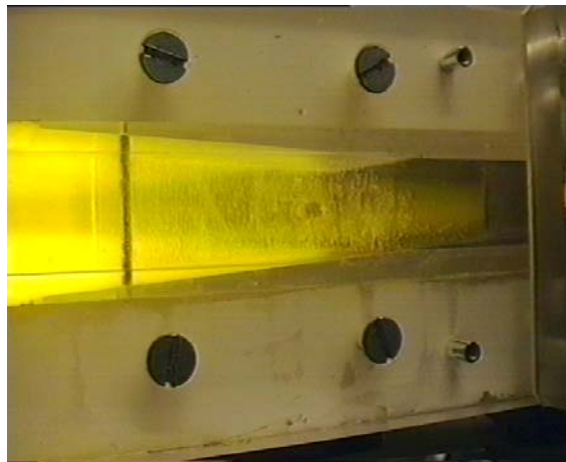


Fig. 13. Photograph of gas channel downstream of the resonator, $n_{\text{He}} = 98 \text{ mmol s}^{-1}$, $n_{\text{Cl}_2} = 33 \text{ mmol s}^{-1}$, $n_{\text{NO}^+} = 0 \text{ mmol s}^{-1}$, $n_{\text{HI}} = 1.7 \text{ mmol s}^{-1}$, $n_{\text{ClO}_2} = 0 \text{ mmol s}^{-1}$

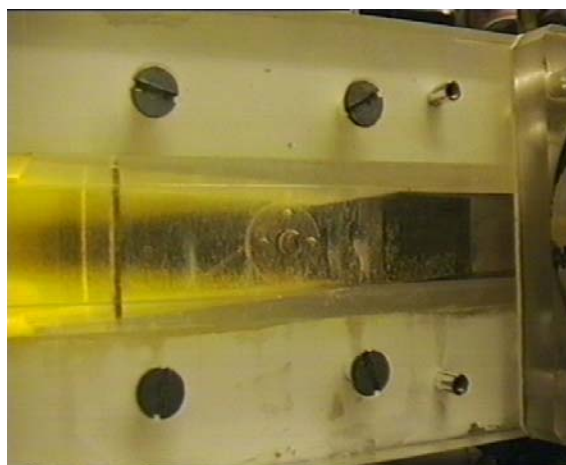


Fig. 14. Photograph of gas channel downstream of the resonator, $n_{\text{He}} = 88 \text{ mmol s}^{-1}$, $n_{\text{Cl}_2} = 33 \text{ mmol s}^{-1}$, $n_{\text{NO}^+} = 4.3 \text{ mmol s}^{-1}$, $n_{\text{HI}} = 1.4 \text{ mmol s}^{-1}$, $n_{\text{ClO}_2} = 0 \text{ mmol s}^{-1}$

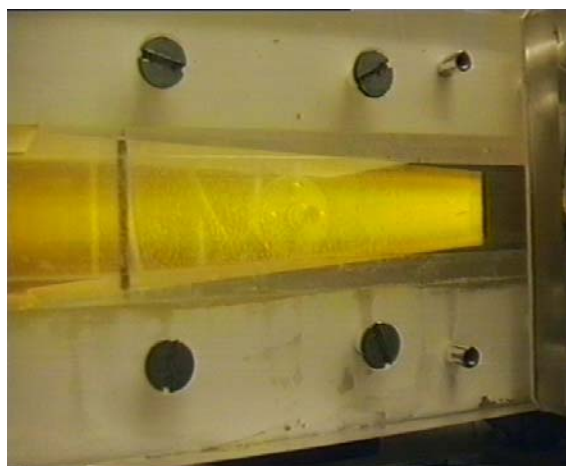


Fig. 15a Photograph of gas channel downstream of the resonator, $n_{\text{He}} = 90 \text{ mmol s}^{-1}$, $n_{\text{Cl}_2} = 33 \text{ mmol s}^{-1}$, $n_{\text{NO}^+} = 4.4 \text{ mmol s}^{-1}$, $n_{\text{HI}} = 2.2 \text{ mmol s}^{-1}$, $n_{\text{ClO}_2} = 1.5 \text{ mmol s}^{-1}$, $P = 375 \text{ W}$

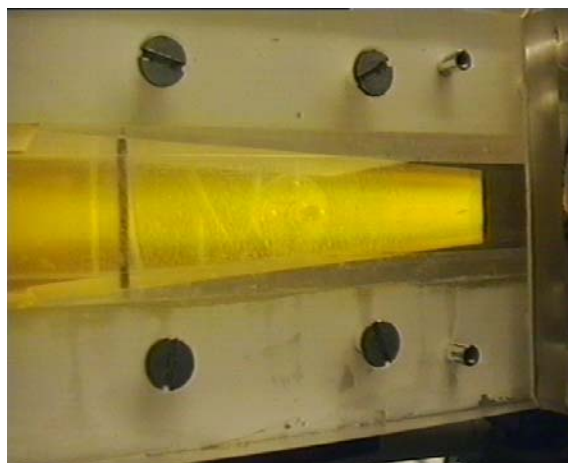


Fig. 15b Photograph of gas channel downstream of the resonator, $n_{\text{He}} = 90 \text{ mmol s}^{-1}$, $n_{\text{Cl}_2} = 40 \text{ mmol s}^{-1}$, $n_{\text{NO}^+} = 4.4 \text{ mmol s}^{-1}$, $n_{\text{HI}} = 2.06 \text{ mmol s}^{-1}$, $n_{\text{ClO}_2} = 1.5 \text{ mmol s}^{-1}$, $P = 430 \text{ W}$

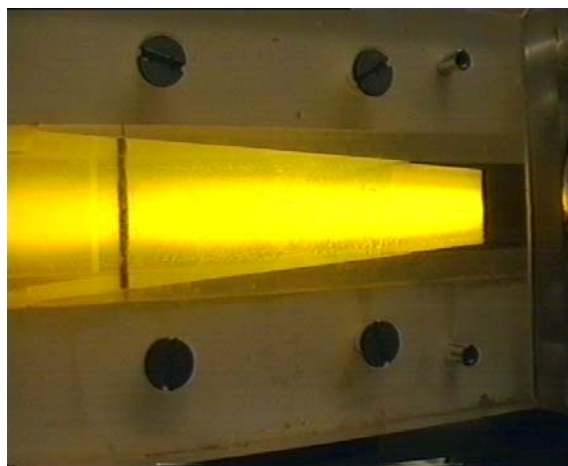


Fig. 16. Photograph of gas channel downstream of the resonator, $n_{\text{He}} = 90 \text{ mmol s}^{-1}$, $n_{\text{Cl}_2} = 40 \text{ mmol s}^{-1}$, $n_{\text{NO}^+} = 2.3 \text{ mmol s}^{-1}$, $n_{\text{HI}} = 2.5 \text{ mmol s}^{-1}$, $n_{\text{ClO}_2} = 1.5 \text{ mmol s}^{-1}$, $P = 280 \text{ W}$



Fig. 17. Beam pattern of COIL at following flow rates (in mmol s^{-1}): $40 \text{ Cl}_2 + 100 \text{ He} + 1.5 \text{ ClO}_2 + 4.9 \text{ NO} + 2.2 \text{ HI}$. Transmissions $T_1 = 0.7 \%$, $T_2 = 0.3 \%$, $P_L = 430 \text{ W}$.

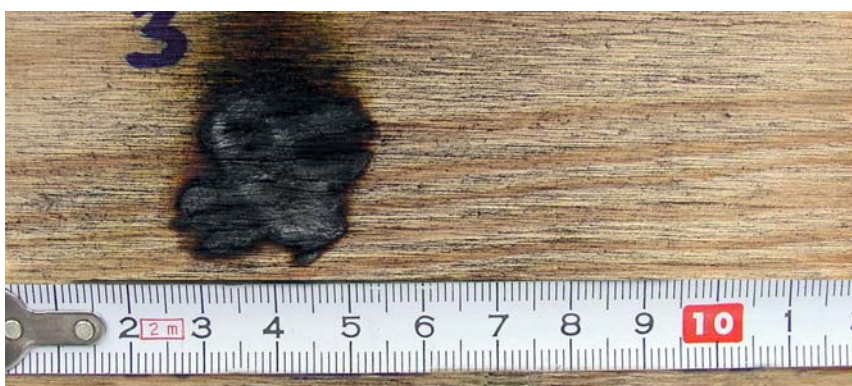


Fig. 18. Beam pattern of COIL at following flow rates (in mmol s^{-1}): $32 \text{ Cl}_2 + 60 \text{ He} + 1.5 \text{ ClO}_2 + 5 \text{ NO} + 1.5 \text{ HI}$. Transmissions $T_1 = 0.7 \%$, $T_2 = 0.3 \%$, $P_L = 120 \text{ W}$.

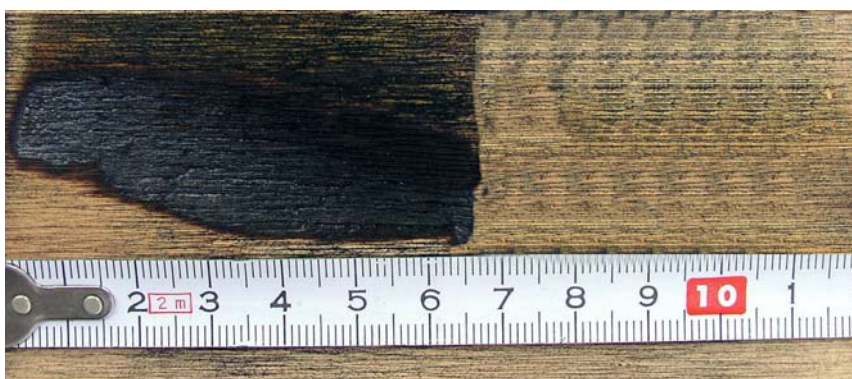


Fig. 19. Beam pattern of COIL at following flow rates (in mmol s^{-1}): $32 \text{ Cl}_2 + 68 \text{ He} + 1.5 \text{ ClO}_2 + 3.3 \text{ NO} + 2 \text{ HI}$. Transmissions $T_1 = 0.7 \%$, $T_2 = 0.3 \%$, $P_L = 330 \text{ W}$.

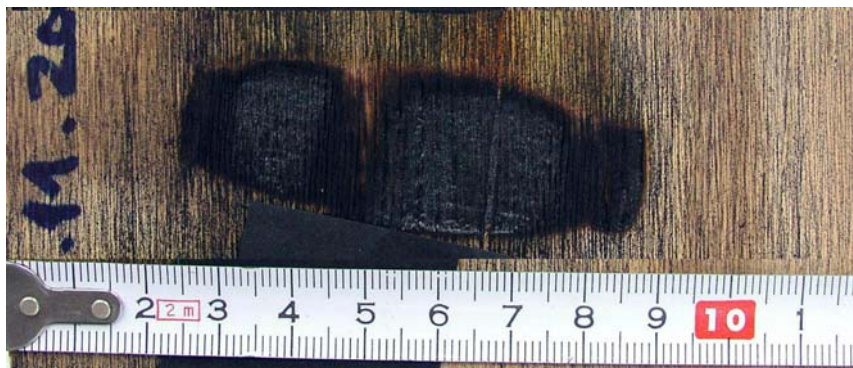


Fig. 20. Beam pattern of COIL at following flow rates (in mmol s^{-1}): $40 \text{ Cl}_2 + 68 \text{ He} + 1.5 \text{ ClO}_2 + 3.3 \text{ NO} + 2 \text{ HI}$. Transmissions $T_1 = 0.7 \%$, $T_2 = 0.3 \%$, $P_L = 330 \text{ W}$.

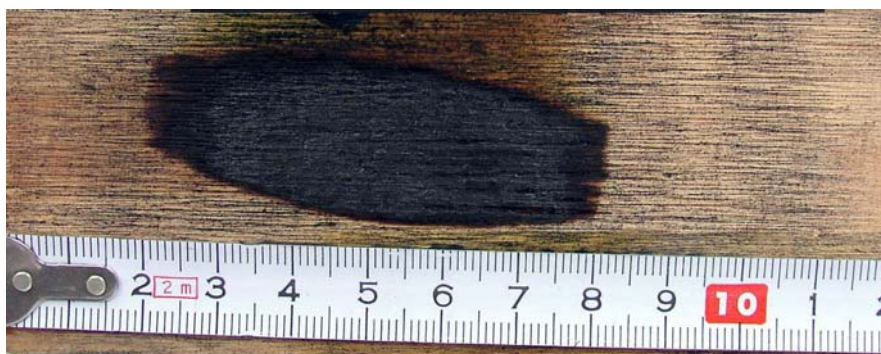


Fig. 21. Beam pattern of COIL at following flow rates (in mmol s^{-1}): $40 \text{ Cl}_2 + 92 \text{ He} + 1.5 \text{ ClO}_2 + 3.3 \text{ NO} + 2 \text{ HI}$. Transmissions $T_1 = 0.7 \%$, $T_2 = 0.3 \%$, $P_L = 330 \text{ W}$.

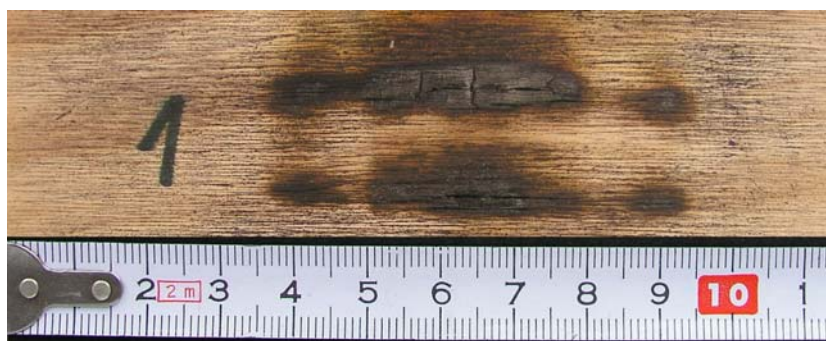


Fig. 22. Beam pattern of COIL at following flow rates (in mmol s^{-1}): $28 \text{ Cl}_2 + 160 \text{ He} + 1 \text{ ClO}_2 + 2 \text{ NO} + 1 \text{ HI}$. Transmissions $T_1 = 0.9 \%$, $T_2 = 0.1 \%$, $P_L = 95 \text{ W}$.

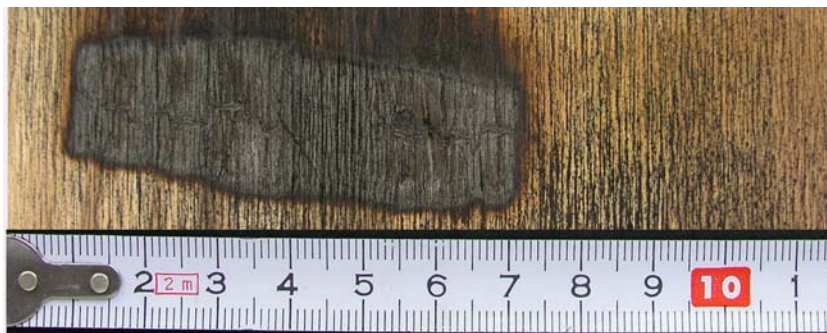


Fig. 23. Beam pattern of COIL at following flow rates (in mmol s^{-1}): $39 \text{ Cl}_2 + 68 \text{ He} + 1 \text{ ClO}_2 + 2.1 \text{ NO} + 2\text{-}3 \text{ HI}$ (10 % HI mixture). Transmissions $T_1 = 0.9 \%$, $T_2 = 0.1 \%$, $P_L = 240 \text{ W}$.



Fig. 24. Beam pattern of COIL at following flow rates (in mmol s^{-1}): $39 \text{ Cl}_2 + 78 \text{ He} + 1.5 \text{ ClO}_2 + 2.75 \text{ NO} + 2\text{-}3 \text{ HI}$ (10 % HI mixture). Transmissions $T_1 = 0.9 \%$, $T_2 = 0.1 \%$, $P_L = 240 \text{ W}$.

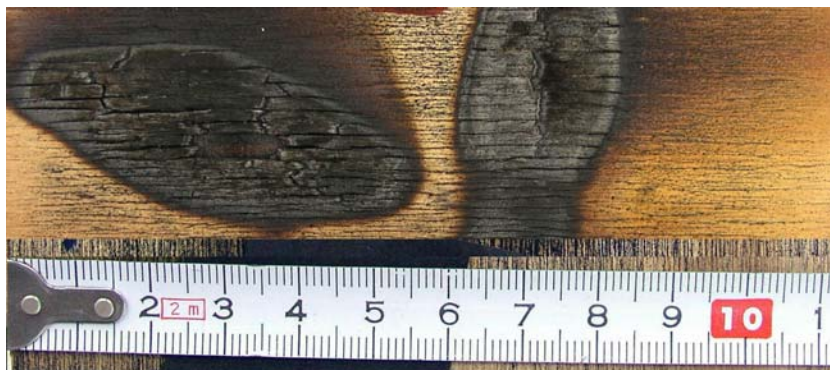


Fig. 25. Beam pattern of COIL at following flow rates (in mmol s^{-1}): $40 \text{ Cl}_2 + 78 \text{ He} + 2.2 \text{ ClO}_2 + 4.2 \text{ NO} + 2\text{-}3 \text{ HI}$ (10 % HI mixture). Transmissions $T_1 = 0.9 \%$, $T_2 = 0.1 \%$, $P_L = 200 \text{ W}$.

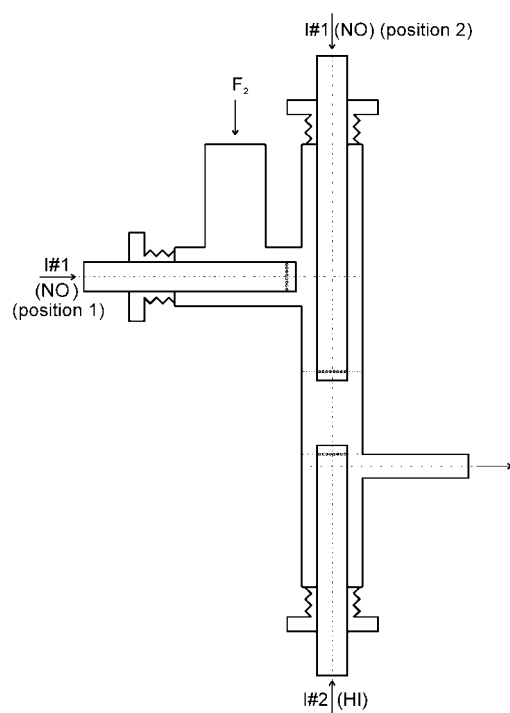


Fig. 26. Cross-section of longitudinal flow reactor with axially movable NO and HI injectors

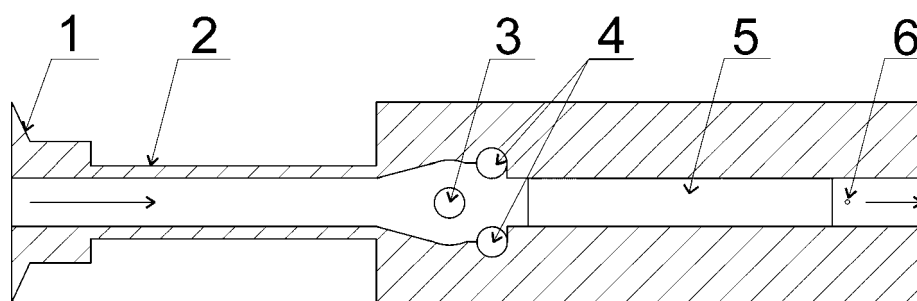


Fig. 27. Cross-section of transverse flow reactor, 1 – input flange, 2 – delta-shaped channel, 3 – NO injector, 4 – HI injectors, 5 – optical cavity for atomic I detection, 6 – thermocouple

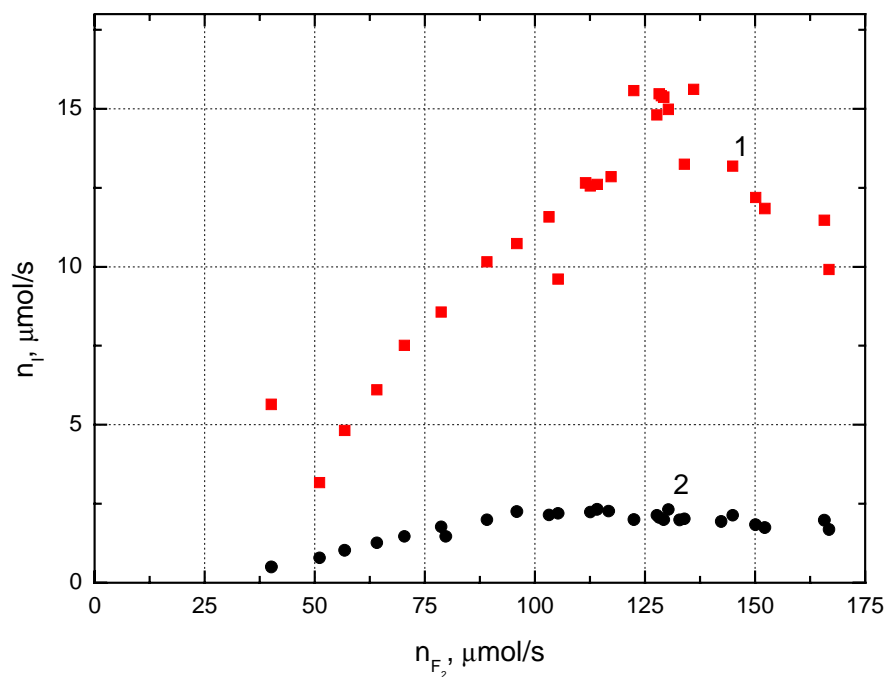


Fig. 28. Flow rate of atomic iodine in dependence on F_2 flow rate; 141 $\mu\text{mol/s}$ NO and 82 $\mu\text{mol/s}$ HI; other conditions the same as in Fig. 5.

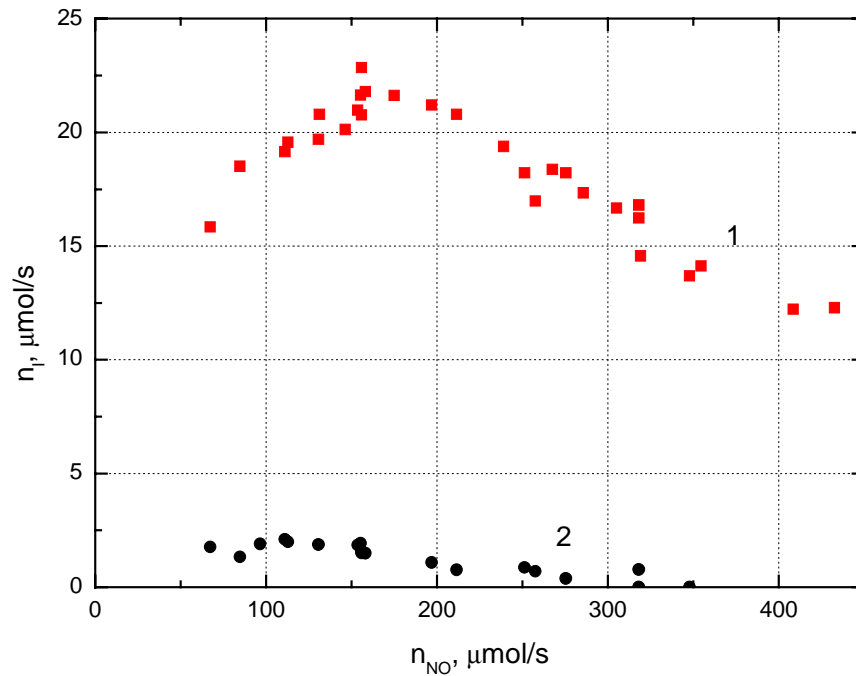


Fig. 29. Flow rate of atomic iodine in dependence on NO flow rate; 155 $\mu\text{mol/s}$ F_2 , 146 $\mu\text{mol/s}$ HI; other conditions the same as in Fig. 5.

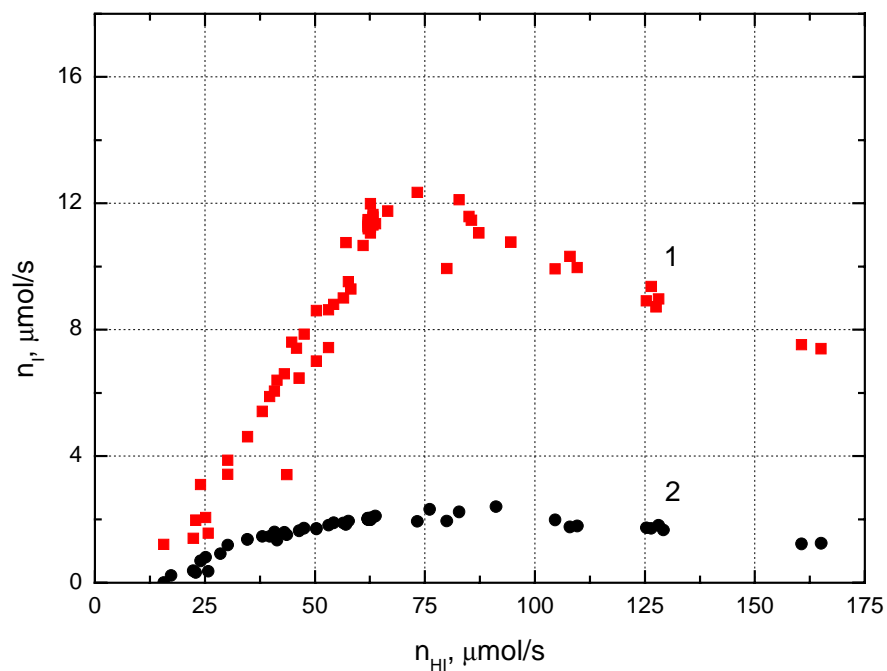


Fig. 30. Flow rate of atomic iodine in dependence on HI flow rate; 105 $\mu\text{mol/s}$ F_2 , 141 $\mu\text{mol/s}$ NO; other conditions the same as in Fig. 5.

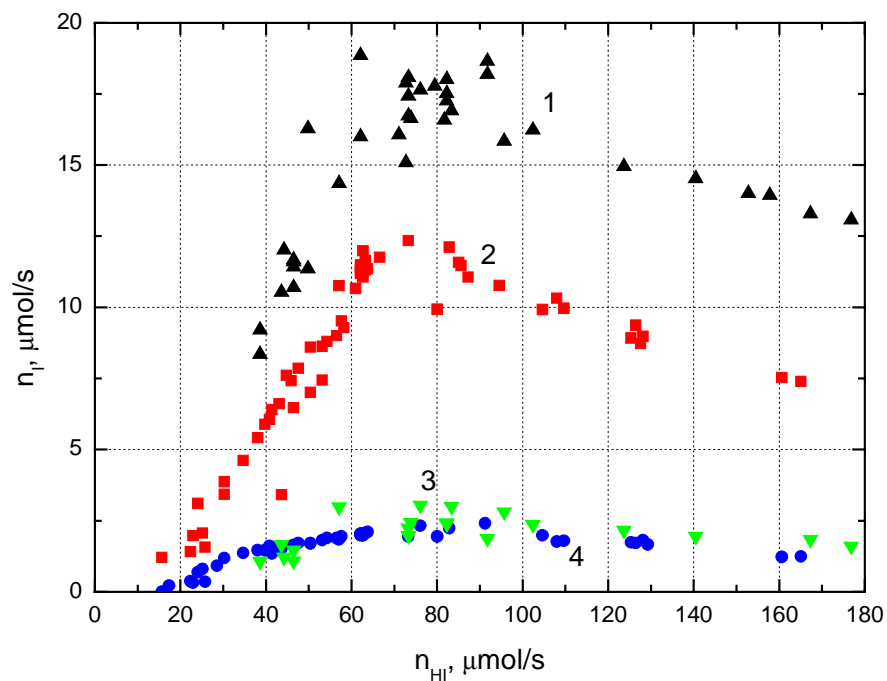


Fig. 31. Flow rate of atomic iodine in dependence on HI flow rate and for different time intervals between HI injection and atomic I detection; 109 $\mu\text{mol/s}$ F_2 , 142 $\mu\text{mol/s}$ NO; τ_{HI-ISD} : 1 – 2.1 ms, 2 – 2.7 ms, 3 – 9.4 ms, and 4 – 10 ms.

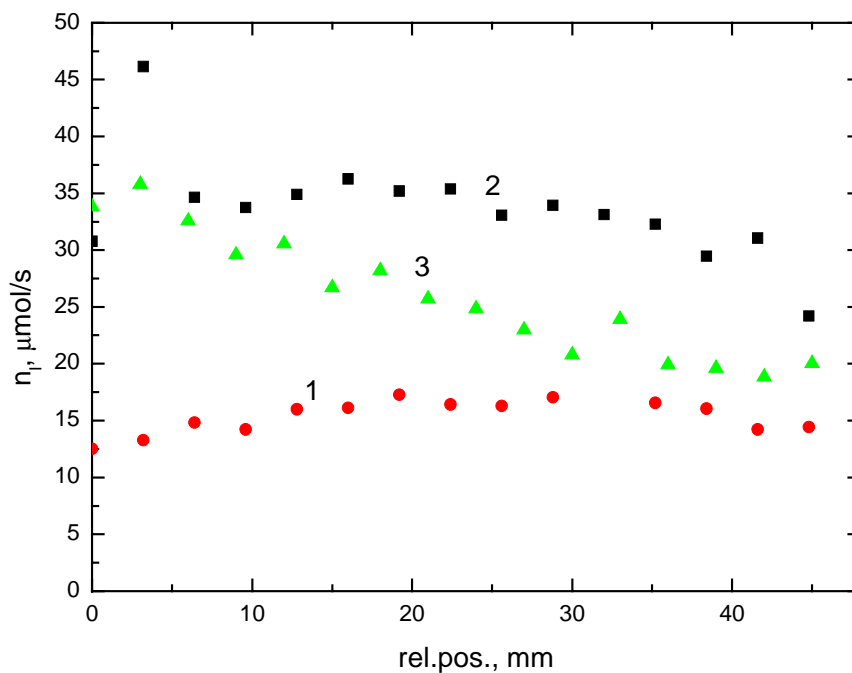


Fig. 32. Concentration profile of atomic iodine along gas flow at different F_2 flow rate, and $221 \mu\text{mol/s}$ NO and $134 \mu\text{mol/s}$ HI; $\tau_{\text{NO-HI}} = 0.18 \text{ ms}$; $\tau_{\text{HI-ISD}} = 0.45 - 2 \text{ ms}$; 1 – $58 \mu\text{mol/s}$ F_2 , 2 – $159 \mu\text{mol/s}$ F_2 , 3 – $277 \mu\text{mol/s}$ F_2 .

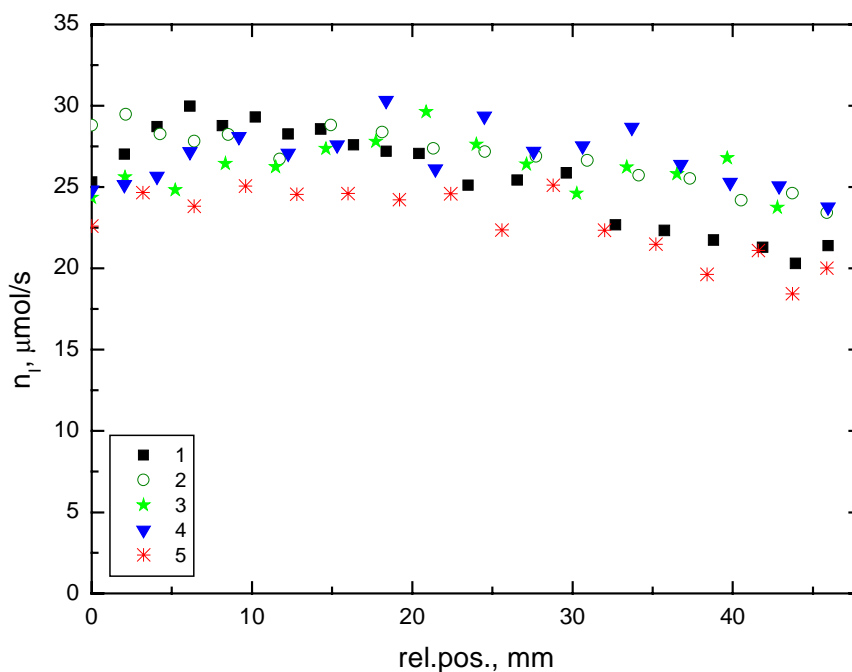


Fig. 33. Concentration profile of atomic iodine along gas flow at different NO flow rate, and $159 \mu\text{mol/s}$ F_2 and $130 \mu\text{mol/s}$ HI; 1 – $104 \mu\text{mol/s}$ NO, 2 – $172 \mu\text{mol/s}$ NO, 3 – $306 \mu\text{mol/s}$ NO, 4 – $371 \mu\text{mol/s}$ NO, 5 – $486 \mu\text{mol/s}$ NO.

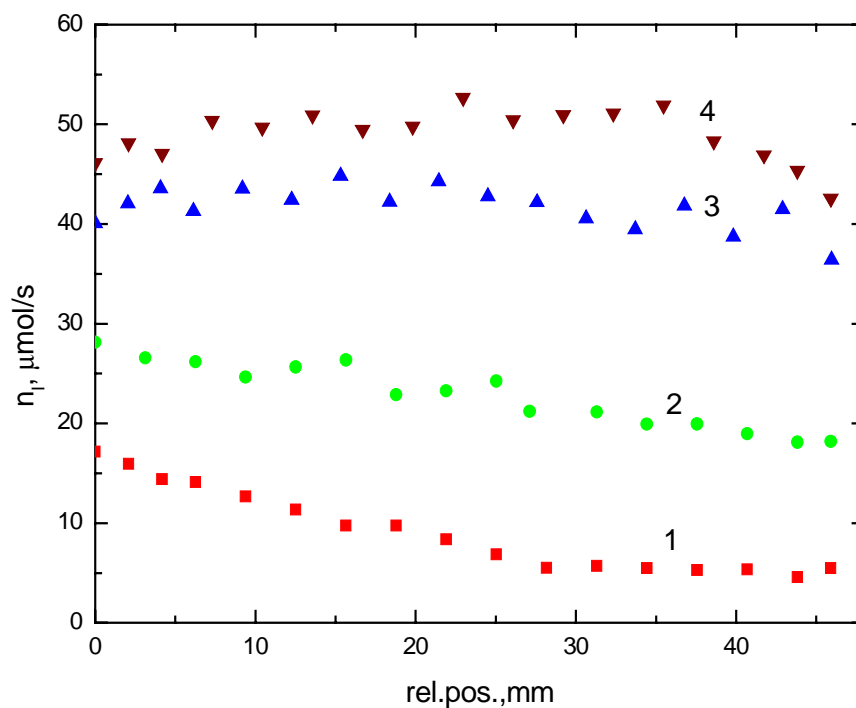


Fig. 34. Concentration profile of atomic iodine along gas flow at different HI flow rate, and 186 $\mu\text{mol/s}$ F_2 and 181 $\mu\text{mol/s}$ NO ; 1 – 61 $\mu\text{mol/s}$ HI, 2 – 128 $\mu\text{mol/s}$ HI, 3 – 225 $\mu\text{mol/s}$ HI, 4 – 472 $\mu\text{mol/s}$ HI

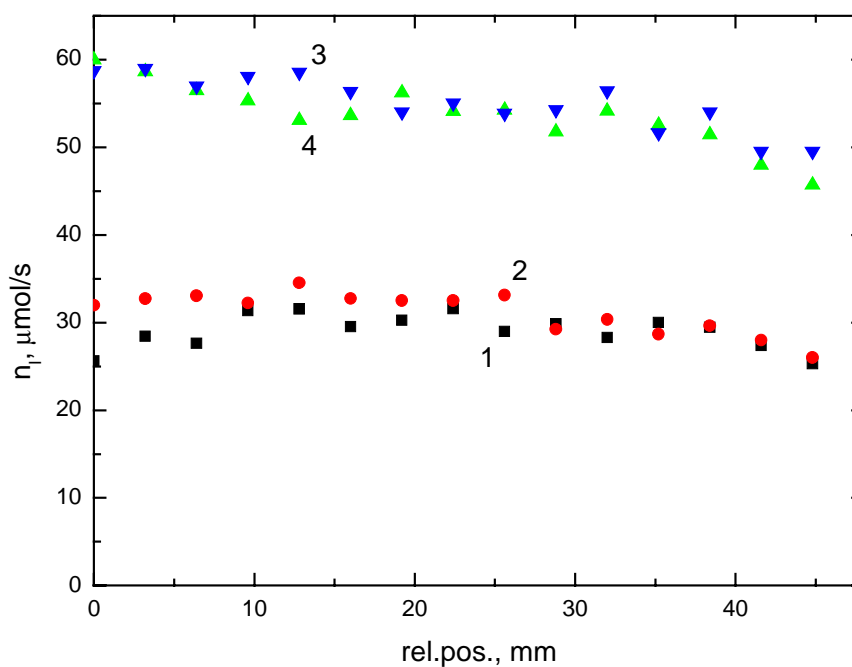


Fig. 35. Concentration profile of atomic iodine along gas flow at different F_2 flow rate, and 312 $\mu\text{mol/s}$ NO and 134 $\mu\text{mol/s}$ HI; 1 – 100 $\mu\text{mol/s}$ F_2 , 2 – 102 $\mu\text{mol/s}$ F_2 , 3 – 260 $\mu\text{mol/s}$ F_2 , 4 – 258 $\mu\text{mol/s}$ F_2 ; other conditions the same as in Fig. 15.

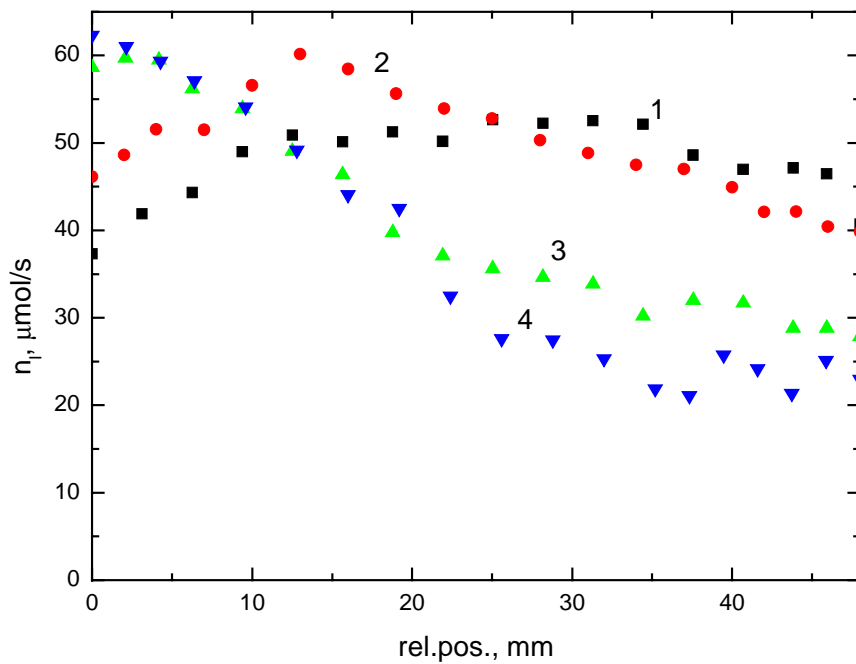


Fig. 36. Concentration profile of atomic iodine along gas flow at different F_2 flow rate, and $94 \mu\text{mol/s}$ HI and $381 \mu\text{mol/s}$ NO; order of HI and NO injection: HI-NO; 1 – $153 \mu\text{mol/s}$ F_2 , 2 – $195 \mu\text{mol/s}$ F_2 , 3 – $267 \mu\text{mol/s}$ F_2 , 4 – $343 \mu\text{mol/s}$ F_2 .

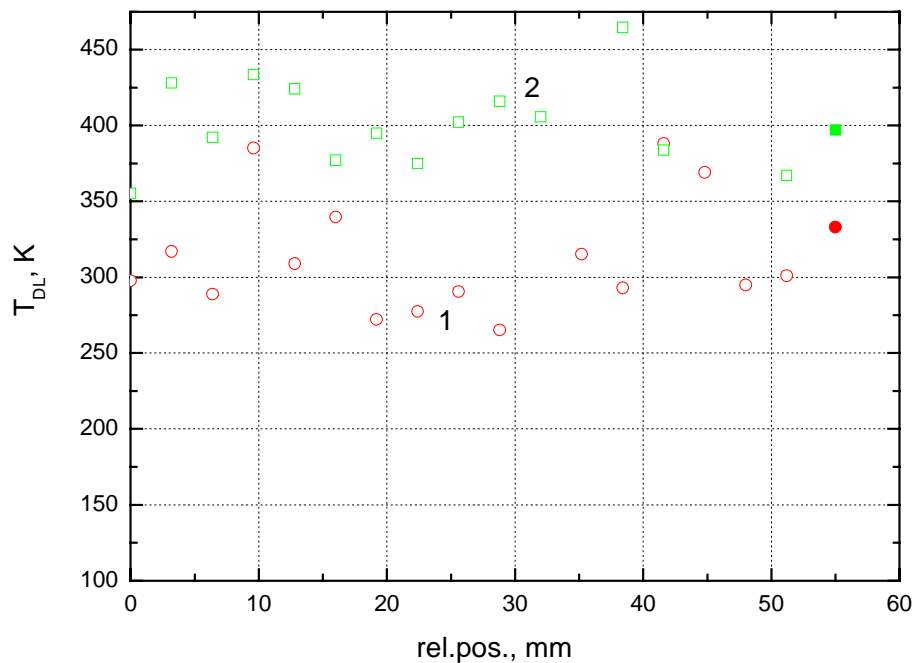


Fig. 37. Temperature of reaction mixture measured by thermocouple (filled symbols) and evaluated from ISD data (corresponding with experimental results in Fig. 32, curve 1 and 2).

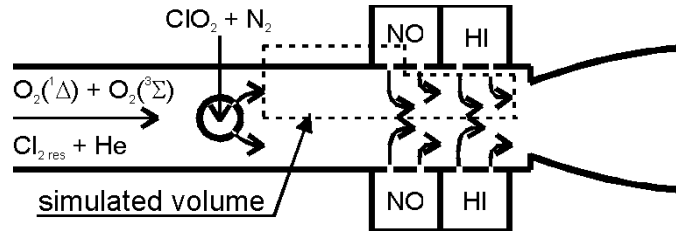


Fig. 38. Mixing nozzle and simulated volume

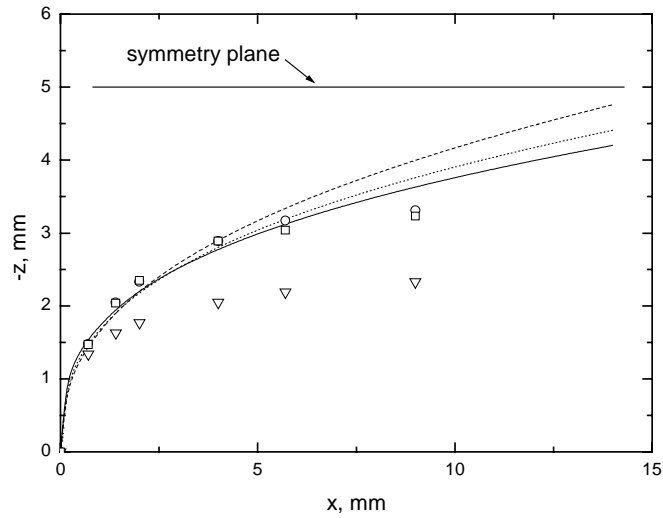


Fig. 39. Penetration depths and locations of NO_{\max} concentration for the Model case 1. Jet axis simulated for laminar (circles) and LES (squares) viscosity formulation. Lines: NO_{\max} concentration from simulation (triangles), represent equations A1 (solid), A2 (dash) and K (dot).

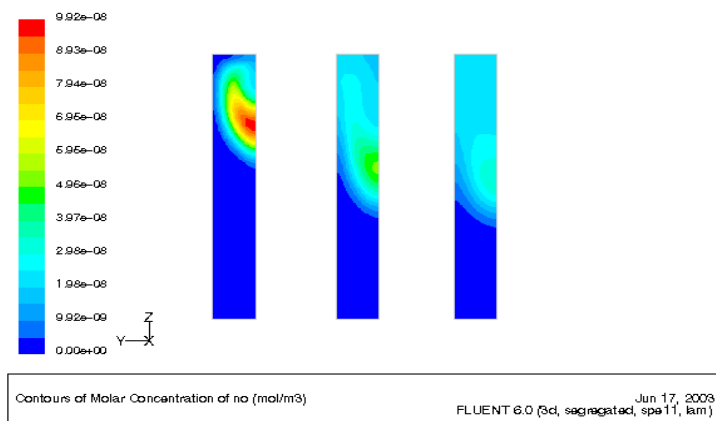


Fig. 40. Contours of NO concentration at $x = 0.7, 5.7$ and 13 mm for the Model case 1. Laminar results.

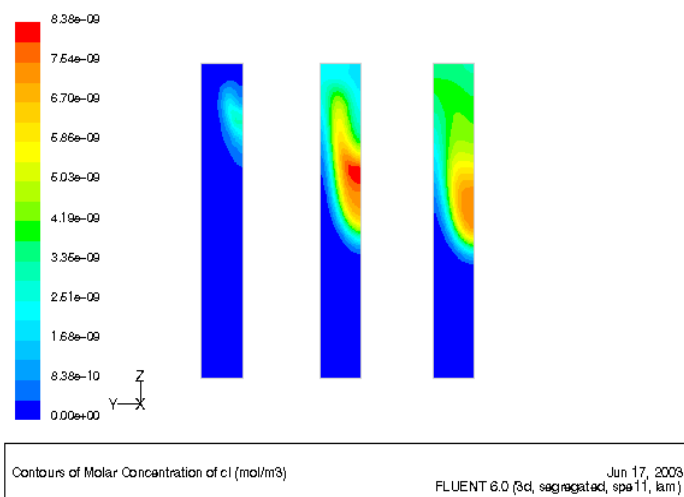


Fig. 41a. Contours of Cl concentration at $x = 0.7, 5.7$ and 13 mm for the Model case 2.

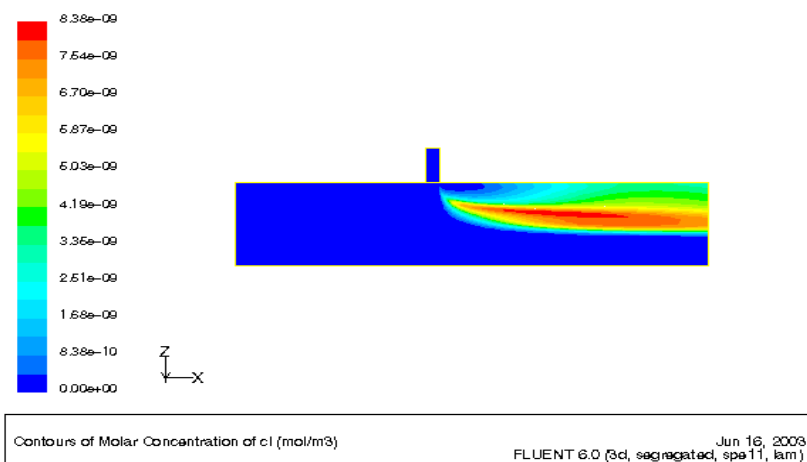


Fig. 41b. Contours of Cl concentration at $xz, y = 0$ plane for the Model case 2.

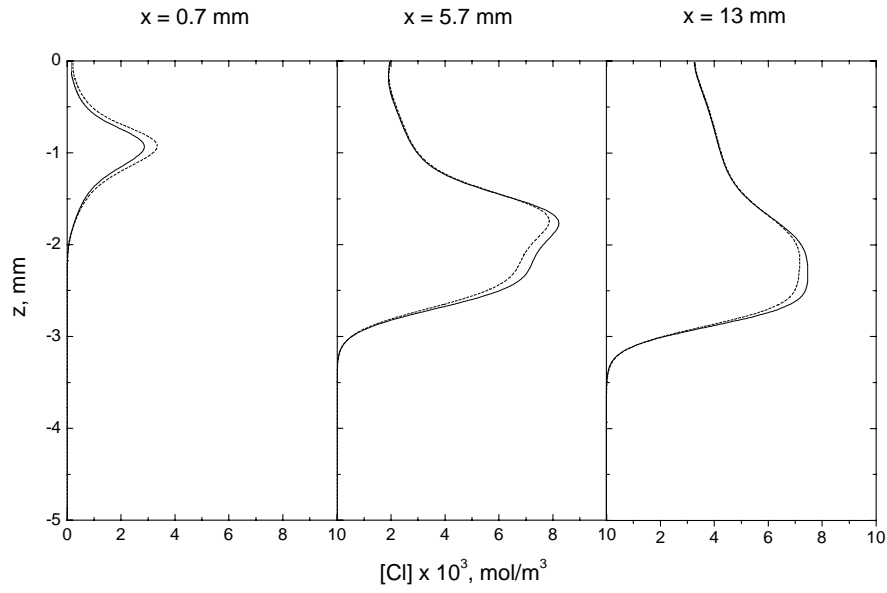


Fig. 42. NO concentration at $y = 0$ and $x = 0.7, 5.7, 13$ mm for the Model case 2. Fick's law results (solid) and Stefan-Maxwell results (dash).

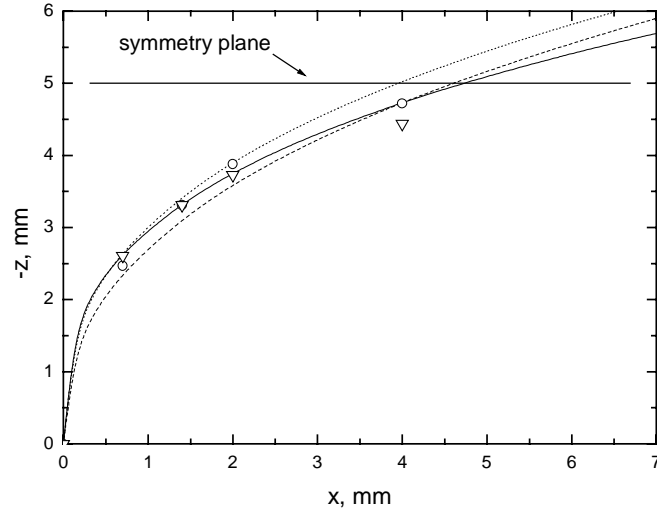


Fig. 43. Penetration depths and locations of NO_{max} concentration for the Model case 3. Jet axis simulated for laminar (circles) viscosity formulation. Lines represent equations A1 (solid), A2 (dash) and K (dot). NO_{max} concentration from simulation (triangles).

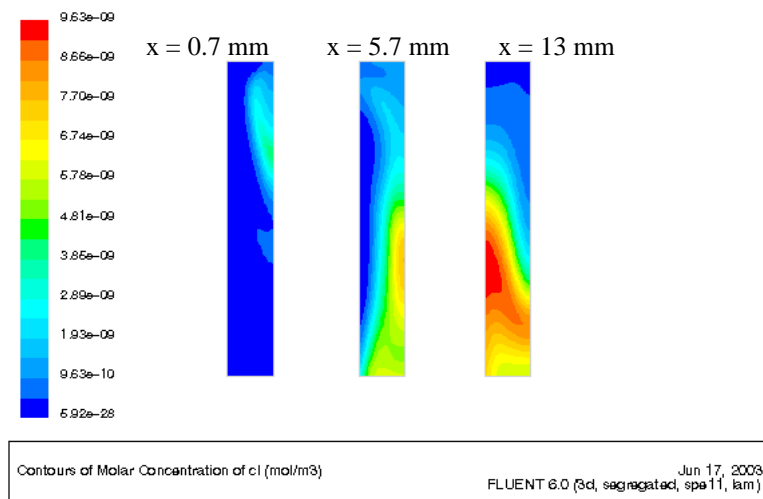


Fig. 44a. Contours of Cl concentration at $x = 0.7, 5.7$ and

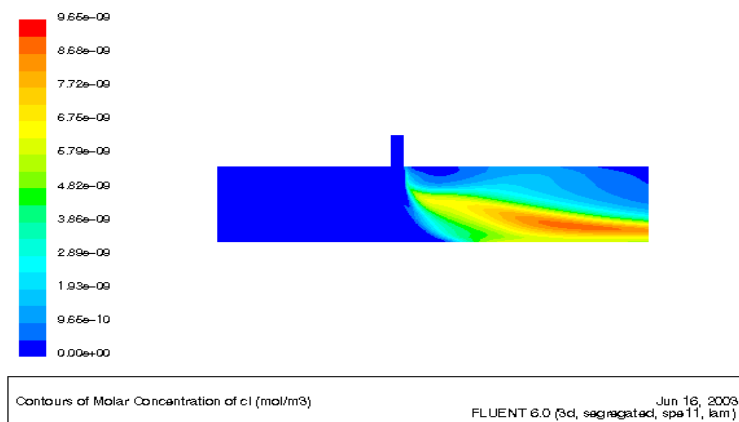


Fig. 44b. Contours of Cl concentration at $xz, y = 0$ plane for the Model case 4.

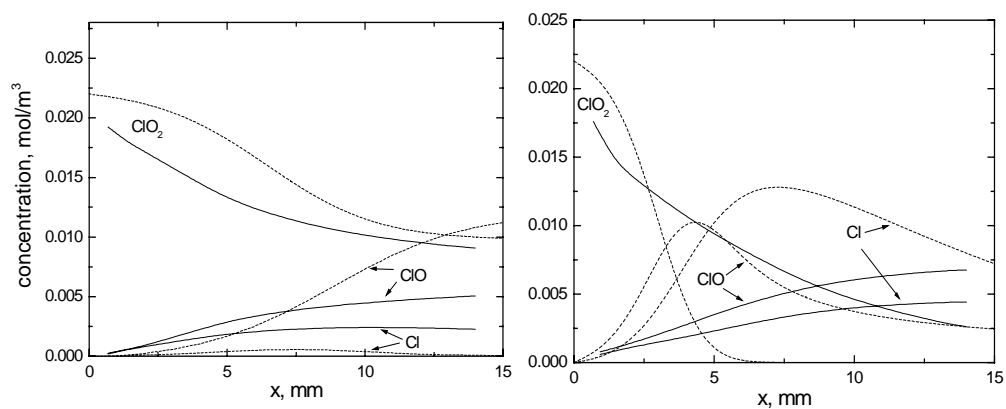


Fig. 45a,b. Comparison between 1-D (dash) and 3-D (solid) calculations of Cl and ClO concentrations for the Model case 2 (a) and Model case 4 (b).

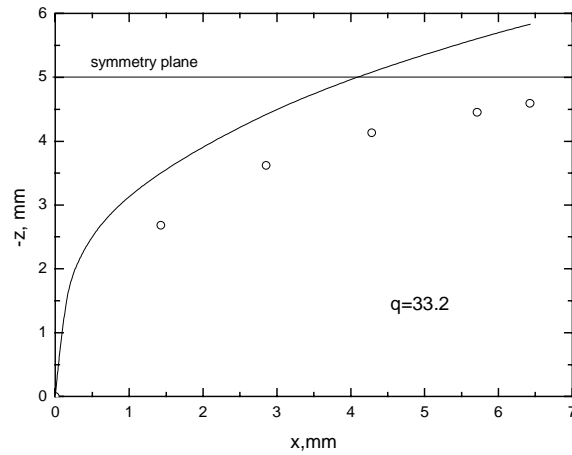


Fig. 46. Penetration depths for the NO large injector (circles). Line represents equation (4)

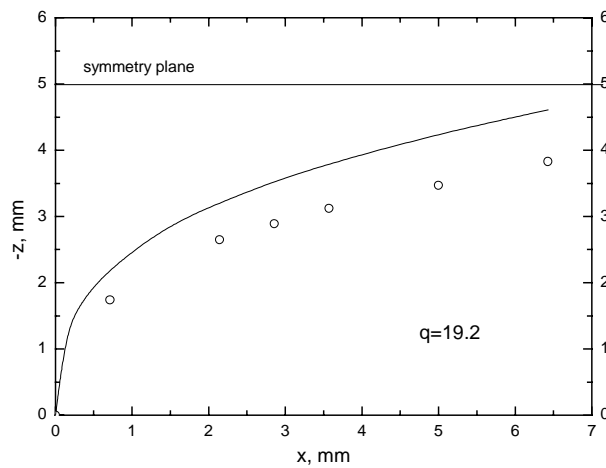


Fig. 47. Penetration depths for the HI large injector (circles). Line represents equation (4)

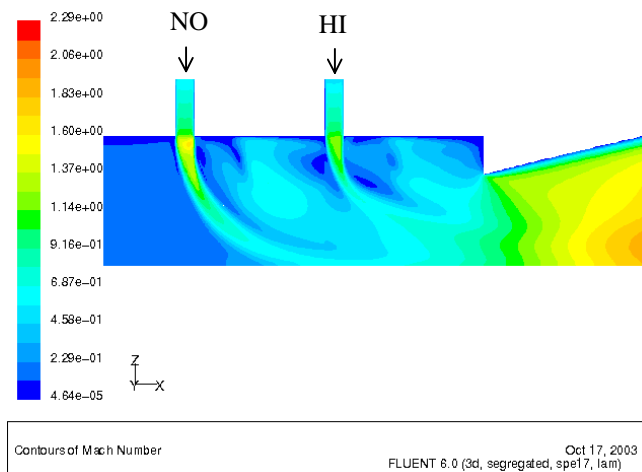


Fig. 48. Contours of Mach number in the vicinity of large injectors

REPORT DOCUMENTATION PAGE				Form Approved OMB No. 0704-0188	
Public reporting burden for this collection of information is estimated to average 1 hour per response, including the time for reviewing instructions, searching existing data sources, gathering and maintaining the data needed, and completing and reviewing the collection of information. Send comments regarding this burden estimate or any other aspect of this collection of information, including suggestions for reducing the burden, to Department of Defense, Washington Headquarters Services, Directorate for Information Operations and Reports (0704-0188), 1215 Jefferson Davis Highway, Suite 1204, Arlington, VA 22202-4302. Respondents should be aware that notwithstanding any other provision of law, no person shall be subject to any penalty for failing to comply with a collection of information if it does not display a currently valid OMB control number. PLEASE DO NOT RETURN YOUR FORM TO THE ABOVE ADDRESS.					
1. REPORT DATE (DD-MM-YYYY) 27-01-2004		2. REPORT TYPE Final Report		3. DATES COVERED (From – To) 16 September 2002 - 16-Sep-03	
4. TITLE AND SUBTITLE Investigation of chemical generation of atomic iodine for a COIL, and its testing in the supersonic COIL, using a diode probe.				5a. CONTRACT NUMBER FA8655-02-M4040	
				5b. GRANT NUMBER	
				5c. PROGRAM ELEMENT NUMBER	
6. AUTHOR(S) Dr. Jarmila Kodymova				5d. PROJECT NUMBER	
				5d. TASK NUMBER	
				5e. WORK UNIT NUMBER	
7. PERFORMING ORGANIZATION NAME(S) AND ADDRESS(ES) Academy of Sciences Na Slovance 2 Prague 8 182 21 Czech Republic				8. PERFORMING ORGANIZATION REPORT NUMBER N/A	
9. SPONSORING/MONITORING AGENCY NAME(S) AND ADDRESS(ES) EOARD PSC 802 BOX 14 FPO 09499-0014				10. SPONSOR/MONITOR'S ACRONYM(S)	
				11. SPONSOR/MONITOR'S REPORT NUMBER(S) SPC 02-4040	
12. DISTRIBUTION/AVAILABILITY STATEMENT Approved for public release; distribution is unlimited.					
13. SUPPLEMENTARY NOTES					
14. ABSTRACT This report results from a contract tasking Academy of Sciences as follows: The contractor will investigate the chemical generation of atomic iodine for a Chemical Oxygen-Iodine Laser (COIL). A small pilot device will be used mainly for the study of atomic iodine generation via chemically produced atomic fluorine, while the larger COIL device will be modified to test its operation with atomic iodine generated via chemically produced atomic chlorine in a flow of singlet oxygen. This will be aimed at obtaining the gain on I(2P1/2) – I(2P3/2) laser transition and lasing at 1.315 mm.					
15. SUBJECT TERMS EOARD, gas lasers, oxygen-iodine lasers, Chemical lasers, Laser physics					
16. SECURITY CLASSIFICATION OF:			17. LIMITATION OF ABSTRACT UL	18, NUMBER OF PAGES 61	19a. NAME OF RESPONSIBLE PERSON INGRID J. WYSONG
a. REPORT UNCLAS	b. ABSTRACT UNCLAS	c. THIS PAGE UNCLAS			19b. TELEPHONE NUMBER (Include area code) +44 (0)20 7514 4285